Topology Optimization for the Elasticity Problem

Sintya Esmeralda Serrano De La Torre

Universidad Nacional de Colombia
Facultad de Ciencias
Bogotá, Colombia
2019

Topology Optimization for the Elasticity Problem

Sintya Esmeralda Serrano De La Torre

Tesis de grado presentado como requisito parcial para optar al título de:
Magister en Matemática Aplicada

Director:
Juan Carlos Galvis

Co-Director:
Boyan S. Lazarov

Línea de Investigación:
Matemática Aplicada

Universidad Nacional de Colombia
Facultad de Ciencias, Departamento Matemática
Bogotá, Colombia
2019

Dedicatoria

A mi familia y amigos

Agradecimientos

Thanks to Juan and Boyan for their infinite patience, support and dedication in the realization of this project.

Resumen

En este libro vamos a proponer varios precondicionadores para la ecuación de elasticidad. Los precondicionadores están construidos en base los métodos de descomposición de dominios y métodos de multiescala para las ecuaciones de calor y elasticidad. El objetivo de la aplicación de dichos precondicionadores es disminuir la condición de la matriz asociada al problema de elasticidad y el número de iteraciones para llegar a la solución del problema. Además presentaremos el problema de optimización topológica donde aplicaremos los precondicionadores al problema de minimización y haremos varios experimentos para mostrar su utilidad en la solución de este tipo de problemas.

Palabras clave: ecuación de elasticidad, método multiescala, descomposición de dominios, precondicionador de dos niveles de Schwarz, optimización topológica.

Abstract

In this work, we propose several preconditioners for the elasticity equation. The preconditioners are built based on domain decomposition and multiscale methods for the heat and elasticity equations. The main goal of the application of preconditioners is to decrease the condition number of the matrix associated with the elasticity problem and the number of iterations needed to arrive at the solution of the elasticity equation. We also present an elasticity topology optimization problem, where we apply the preconditioners to the minimum compliance design problems. We present numerical experiments in order to show the advantages of our approach to the solution of these type of problems.

Keywords: elasticity problem, multiscale method, domain decomposition method, two level Schwarz prreconditoner, topology optimization.

Contents

List of Figures

List of Tables

1 Introduction

The objective of this document is to obtain an elasticity preconditioner to improve the numerical methods in topology optimization problems. For the topology optimization, we consider the finite element formulation of the elasticity equation in a fine mesh to capture the small details of the design structure. One of the issues of solving the optimization problem with a fine mesh is that the linear system solved in every optimization step is poorly conditioned leading to a high computational cost. For instance, in some articles [3, 1, 22, 23], the authors present problems associated with the design of structures with specific properties for different purposes, if the structure is complex (for instance, the structure has high stiffness channels), we need the fine mesh to capture details in each part of the structure.

An implementation and design of some two-levels preconditioner for the elasticity to solve topology optimization problems is presented in [22]. In this work design numerically test a several model a two-levels preconditioner for the elasticity and also we use the two-levels preconditioner from the heat equation as in [37] based in a work by [20] and [19]. We mix the preconditioners from the heat and elasticity problem and create a preconditioner that improves the condition of the problem and that is cheaper because it has half the size of the two-levels elasticity preconditioner that in two dimensions leads to a reduction of the computational cost by a factor of 4.

The first chapter summarizes the two-dimensional elasticity problem that is used in topology optimization, including the most relevant definitions and the variational formulation with the finite element method of the elasticity problem in a square mesh. We also present some experiments with different material contrast that simulate the structure of materials. The performance of the solvers in these experiments are compared with the two-levels preconditioner in the next chapter.

In the next chapters, we focus on describing the methods to create the elasticity two-levels preconditioner. First we describe the multiscale method for the elasticity equation that uses local information to build smaller dimensional coarse spaces, as in [13, 12, 16, 4]. Then we review the overlapping domain decomposition preconditioner, which uses the coarse space obtained in the multiscale method, as in [30, 10, 17, 18, 14]. After that, we build some preconditioners that uses the two-levels heat preconditioner and the two-levels elasticity preconditioner.

In the fifth chapter we describe the minimization problem of the elasticity equation for the design of certain structures, and the challenges to find a structure that can be built for a desired purpose. In this chapter, we present several numerical examples of topology optimization problems. For each experiment, we use the best preconditioners obtained in the previous chapters and we analyze the performance of different preconditioners comparing the number of iterations and the objective function value with high contrast coefficient.

In the last chapter we present some comments and final conclusions.

2 Elasticity problem

In this part, we introduce the most important constitutive equations of the stress approach for isotropic media under internal or external forces applied to a continuum. We begin with some general remarks about the principles of linear elasticity as defined by Hooke's law see more in [25]. We present the problem of linear elasticity in two dimensions. Then we discretize the elasticity problem in two dimensions and present its variational formulation. We also, show examples of the solution of the elasticity equation with different contrasts.

2.1 Linear elasticity

We consider a three-dimensional isotropic body Ω with Γ boundary. The boundary conditions are defined in two different parts, Γ_1 and Γ_2 with prescribed displacements u and the normal stress σ_n respectively.

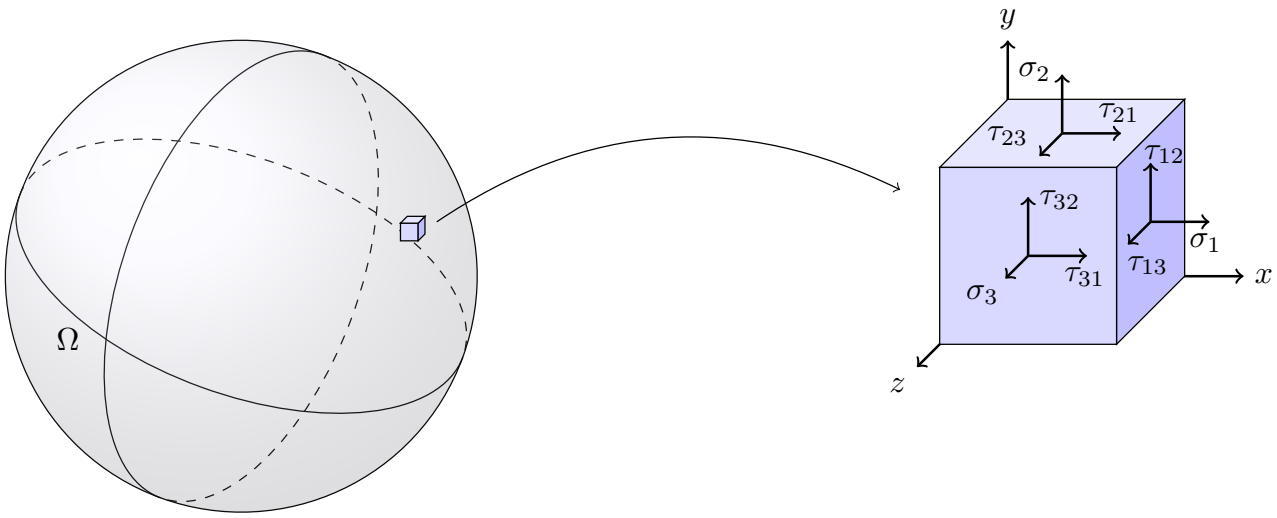

Figure **2-1**: A body Ω under external and internal forces F, boundary divided Γ_1 and Γ_2, normal stress σ_n and the displacement u. And the right picture is the tensor in the infinitesimal element over Ω, with σ_i for $i = 1, 2, 3$. normal stresses and τ_{ij} for $i, j = 1, 2, 3$ the plane stress.

The stress state of internal forces at a point of the body is imagined as an infinitesimal small cube like Figure **2-1**. The stress acting of six sides of the cube can be resolved into components normal to the 2 axes. The stress tensor σ is

$$\sigma = \begin{bmatrix} \sigma_{11} & \tau_{12} & \tau_{13} \\ \tau_{21} & \sigma_{22} & \tau_{23} \\ \tau_{31} & \tau_{32} & \sigma_{33} \end{bmatrix},$$

where σ_{11}, σ_{22} and σ_{33} are the stress components aligned with the x,y, and z axes and τ_{ij} the cubic face i and have j direction. In the engineering literature the tensor's symmetry help us to write the stress tensor with Voigt notation is,

$$\widehat{\sigma} = [\sigma_{11} \quad \sigma_{22} \quad \sigma_{33} \quad \tau_{23} \quad \tau_{13} \quad \tau_{12}]^\top.$$

Which should satisfy the equilibrium's equations

$$\begin{aligned} \frac{\partial \sigma_{11}}{\partial x} + \frac{\partial \tau_{12}}{\partial y} + \frac{\partial \tau_{13}}{\partial z} + F_x = 0, \\ \frac{\partial \sigma_{22}}{\partial y} + \frac{\partial \tau_{12}}{\partial x} + \frac{\partial \tau_{23}}{\partial z} + F_y = 0, \\ \frac{\partial \sigma_{33}}{\partial z} + \frac{\partial \tau_{13}}{\partial x} + \frac{\partial \tau_{23}}{\partial y} + F_z = 0. \end{aligned}$$

F_x, F_y and F_z are the volume load's components, see more in [33], and the equilibrium's equation is

$$-\operatorname{div}(\sigma) = F. \tag{2-1}$$

We can write the stress tensor in the Voigt notation as

$$-\widehat{\nabla}^\top(\widehat{\sigma}) = F, \tag{2-2}$$

where

$$\widehat{\nabla} = \begin{bmatrix} \frac{\partial}{\partial x} & 0 & 0 \\ 0 & \frac{\partial}{\partial y} & 0 \\ 0 & 0 & \frac{\partial}{\partial z} \\ 0 & \frac{\partial}{\partial z} & \frac{\partial}{\partial y} \\ \frac{\partial}{\partial z} & 0 & \frac{\partial}{\partial x} \\ \frac{\partial}{\partial y} & \frac{\partial}{\partial x} & 0 \end{bmatrix}.$$

When an elastic body is subjected to loading, it changes size and displaces, then the relative deformations are called strain. The strain is a relative change of a dimension of a body and in the three-dimensional body is defined by the so-called strain tensor given as,

$$\varepsilon = \begin{bmatrix} \varepsilon_{11} & \gamma_{12} & \gamma_{13} \\ \gamma_{21} & \varepsilon_{22} & \gamma_{23} \\ \gamma_{31} & \gamma_{32} & \varepsilon_{33} \end{bmatrix},$$

$ij(kl)$	$I(J)$
11	1
22	2
33	3
$23, 32$	4
$13, 31$	5
$12, 21$	6

Table **2-1**: Voigt notation for the stiffness matrix, see [21]. In the left column are the pair indexes of the stiffness tensor C and in the right column are the replace indexes that reduce the tensor.

in the reduced notation the tensor ε has six independent components,

$$\widehat{\varepsilon} = [\varepsilon_{11} \quad \varepsilon_{22} \quad \varepsilon_{33} \quad \gamma_{23} \quad \gamma_{13} \quad \gamma_{12}]^\top .$$

In the so-called small displacement theory the strain-displacement tensor is given as follows

$$\varepsilon(u) = \frac{1}{2}\left(\nabla u + (\nabla u)^\top\right), \tag{2-3}$$

where u is the displacement of the point of isotropic media.

In addition to the equilibrium and kinematic equations defined above, we need the constitutive equations providing the link between stress and strain,

$$\sigma = C\varepsilon(u) \tag{2-4}$$

where C contains the constitutive parameters (Young's modulus, bulk modulus and Poisson's ratio) and C is a fourth-rank tensor usually called stiffness tensor with 81 entries.

$$\sigma_{ij} = \sum_{k=1}^{3}\sum_{l=1}^{3} C_{ijkl}\varepsilon_{kl}, \qquad \text{with} \qquad i, j, k, l \in \{1, 2, 3\}. \tag{2-5}$$

Due to symmetries in the tensor C_{ijkl} would be written in the 6×6 stiffness matrix C_{IJ} [21]. This means the couple of indexes $ij(kl)$ are replaced by one index $I(J)$ according to the next table In the most simple symmetry case of the isotropic elastic material depends of Young's modulus E and Poisson's ratio ν (measure of a material tends to expand in directions perpendicular to the direction of compression see more in [21]). The stiffness tensor C_{ijkl} can be written like,

$$C_{ijkl} = \left[\frac{E\nu}{3(1+\nu)(1-2\nu)}\delta_{ij}\delta_{kl} + \frac{E}{2(1+\nu)}(\delta_{ik}\delta_{jl} + \delta_{il}\delta_{jk})\right]\varepsilon_{kl}, \tag{2-6}$$

where δ is the Kronecker delta function defined as

$$\delta_{ij} = \begin{cases} 0 & \text{for} \quad i \neq j \\ 1 & \text{for} \quad i = j \end{cases}, \quad i, j \in \{1, 2, 3\}.$$

And the stiffness tensor of isotropic media in Voigt notation is

$$C = \begin{pmatrix} C_{33} & C_{12} & C_{12} & 0 & 0 & 0 \\ C_{12} & C_{33} & C_{12} & 0 & 0 & 0 \\ C_{12} & C_{12} & C_{33} & 0 & 0 & 0 \\ 0 & 0 & 0 & C_{55} & 0 & 0 \\ 0 & 0 & 0 & 0 & C_{55} & 0 \\ 0 & 0 & 0 & 0 & 0 & C_{55} \end{pmatrix}.$$

We can combine the equilibrium's equation (2-1), strain-displacement tensor defined in (2-3) and the Hooke's law (2-4) for a isotropic media, in the first order differential equation

$$\begin{cases} -\operatorname{div}(\sigma) &= F, \\ \sigma - C(\varepsilon(u)) &= 0. \end{cases} \tag{2-7}$$

The last equation system can be combined in a second order equation

$$-\operatorname{div}(C(\varepsilon(u))) = F. \tag{2-8}$$

For plane bodies with loads applied in-plane the 3D problem is reduced to 2D with details provided in the next section.

2.2 Two dimension elasticity problem

To study the elasticity in two dimensions, discuss two cases: plane stress and plane strain. For the **plane stress**, we consider a thin plate, as in Figure **2-2**(a), wherein the loading is uniformly distributed over the thickness, parallel to the plane of the plate. And for the **plane strain** we consider a cylinder under pressure and assume the external force to be functions of the x and y coordinates only see in Figure **2-2**(c). In both cases, we just analyze the body in the $xy-$plane, as in [25, 31].

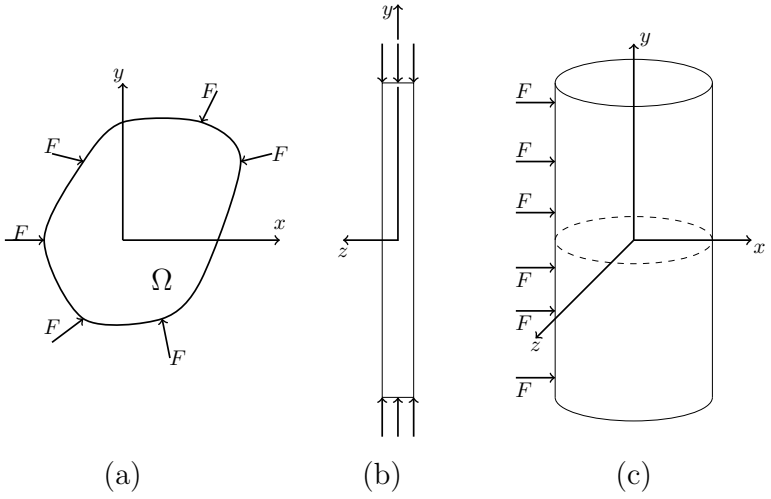

Figure **2-2**: Figure (a), represent the plane stress problem with load forces F applied perpendicular to the z direction. Figure (b), shows the forces when the body is projected in the yz plane and Figure (c), is the plane deformation problem when the load forces are perpendicular to the $xy-$plane.

We work on a body made of an isotropic linear elastic material, with a boundary Γ divided into two parts, Γ_u and Γ_σ with prescribed displacements u, traction forces σ_n respectively and load force F like in Figure **2-3**.

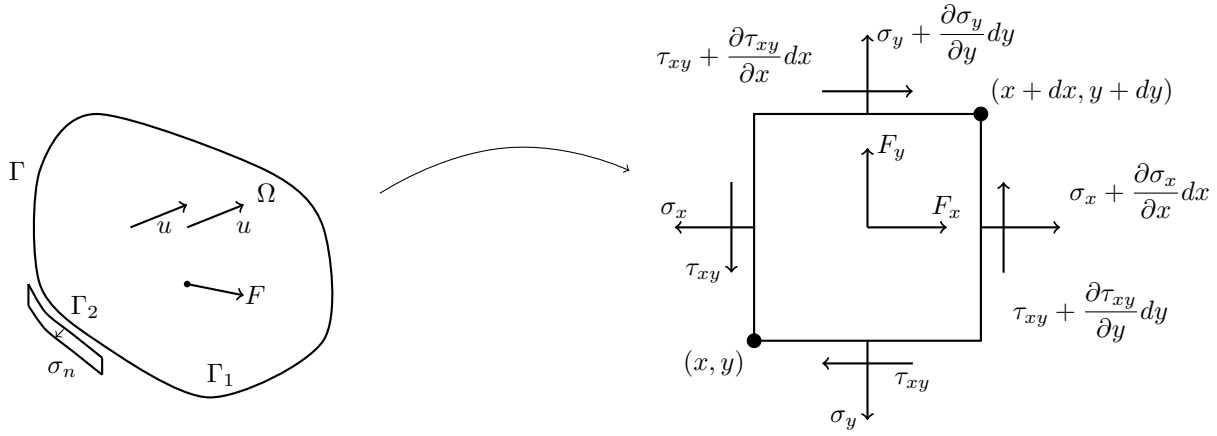

Figure **2-3**: Domain Ω over the xy-plane with loading force F and boundary Γ. The boundary is divided in two sub-boundaries Γ_1 and Γ_2. The displacement u and normal stress σ_n is the prescribed over Γ_2.

The stress state at a point of the body is defined by

$$\sigma = \begin{bmatrix} \sigma_{11} & \tau_{12} \\ \tau_{21} & \sigma_{22} \end{bmatrix},$$

where σ_{11} and σ_{22} are the normal stress components in the x and y direction and τ_{12} is the plane stress and represent the shear stress in the cubic face x that have y direction. Note also that $\tau_{12} = \tau_{21}$, using this symmetry we can write the stress tensor with Voigt notation (reduce tensor dimension):

$$\widehat{\sigma} = [\sigma_{11} \quad \sigma_{22} \quad \tau_{12}]^\top.$$

In the plane stress problem and plane deformation, the stress in the z plane and z direction are insignificant. The stress should satisfy the equilibrium's equations

$$\frac{\partial \sigma_{11}}{\partial x} + \frac{\partial \tau_{12}}{\partial y} + F_x = 0,$$
$$\frac{\partial \sigma_{22}}{\partial y} + \frac{\partial \tau_{12}}{\partial x} + F_y = 0,$$

whereF_x and F_y are the volume load's components in two dimension problem is not considered because the changes in the stress components in the z axes are small than changes in the x, y axes, see more in [33].

If we write in the Voigt notation, see more in [21], the equilibrium's equation is,

$$-\widehat{\nabla}^\top(\widehat{\sigma}) = F, \tag{2-9}$$

where

$$\widehat{\nabla} = \begin{bmatrix} \frac{\partial}{\partial x} & 0 \\ 0 & \frac{\partial}{\partial y} \\ \frac{\partial}{\partial y} & \frac{\partial}{\partial x} \end{bmatrix}.$$

Also we define the strain tensor at a point of the body, by

$$\varepsilon = \begin{bmatrix} \varepsilon_{11} & \gamma_{12} \\ \gamma_{21} & \varepsilon_{22} \end{bmatrix},$$

or in compact notation as,

$$\widehat{\varepsilon} = [\varepsilon_{11} \quad \varepsilon_{22} \quad \gamma_{12}]^\top.$$

In the small displacement theory, the strain-displacement are given by the strain tensor as in (2-3) and the constitutive equation is given by (2-4), but in two dimension elasticity, stiffness tensor C is a fourth-rank tensor usually called stiffness tensor and which has 16 entries.
In general, form Hooke's Law reads,

$$\sigma_{ij} = \sum_{k=1}^{2}\sum_{l=1}^{2} C_{ijkl}\varepsilon_{kl}, \qquad \text{with} \qquad i,j,k,l \in \{1,2\}. \tag{2-10}$$

The Hooke's law leads to complicated relations but simplifies in the isotropic media case, see more in [21]. Each component of stress σ_{ij} is linearly dependent upon every components of strain ε_{kl}.
On the other hand, one way to express the strain as a linear combination stress

$$\varepsilon_{ij} = \sum_{k=1}^{2}\sum_{l=1}^{2} C_{ijkl}\sigma_{kl}, \qquad i,j \in \{1,2\}, \tag{2-11}$$

where (D_{ijkl}) is the elastic compliance tensor and its elements are called compliances. Note that and D and C have the same symmetry and

$$C_{ijkl}D_{klmn} = I_{ijmn}.$$

The stiffness tensor C_{ijkl} would be written in the 4×4 stiffness matrix C_{IJ}, see more in [21]. This means that the couple of indexes $ij(kl)$ are replaced by one index $I(J)$ according to the table **2-2**, see more in [21].

$ij(kl)$	$I(J)$
11	1
22	2
12, 21	3

Table **2-2**: Voigt notation for the stiffness matrix in two dimensions. In the left column are the pair indexes of the stiffness tensor C and in the right column are the indexes that we must replace to reduce the tensor.

For the plane stress we define the stiffness tensor in the isotropic media like,

$$C(x) = \frac{E}{1-\nu^2}\begin{pmatrix} 1 & \nu & 0 \\ \nu & 1 & 0 \\ 0 & 0 & \frac{1-\nu}{2} \end{pmatrix},$$

where E is the Young's modulus and ν is Poisson's ratio, see more in [25]. And for a plane deformation state we have

$$C(x) = \frac{E(1-\nu)}{(1+\nu)(1-2\nu)}\begin{pmatrix} 1 & \frac{\nu}{1-\nu} & 0 \\ \frac{\nu}{1-\nu} & 1 & 0 \\ 0 & 0 & \frac{1-2\nu}{2(1-\nu)} \end{pmatrix}.$$

We can combine equations (2-1), (2-3) and (2-4) in the first order differential equation:

$$\begin{cases} -\operatorname{div}(\sigma) & = F, \\ \sigma - C(x)(\varepsilon(u)) & = 0. \end{cases} \tag{2-12}$$

This problem can also be written as the second order equation

$$-\operatorname{div}(C(x)(\varepsilon(u))) = F. \tag{2-13}$$

2.3 Two dimension elasticity variational formulation

Equation (2-8) represents the elasticity problem in two dimensions. We obtained the variational formulation by introducing an arbitrary virtual displacement v in (2-8) and integrating the terms over the domain Ω

$$\int_\Omega -\operatorname{div}(C(x)(\varepsilon(u))) : v \, d\,\Omega = \int_\Omega F : v \, d\,\Omega,$$

where : represent the Frobenius product, which is a component-wise inner product of two matrices, see in [35].

And using Green's Formula, we have

$$\int_\Omega (C(x)(\varepsilon(u))) : \varepsilon(v) \, d\,\Omega - \int_\Gamma \sigma_n : v \, d\,S = \int_\Omega F : v \, d\,\Omega,$$

and

$$\int_\Omega (C(x)(\varepsilon(u))) : \varepsilon(v) \, d\,\Omega = \int_\Omega F : v \, d\,\Omega + \int_\Gamma \sigma_n : v \, d\,S. \tag{2-14}$$

In the Voigt notation (2-14) can be written

$$\int_\Omega \widehat{\varepsilon}^\top(v)\widehat{C}(x)\widehat{\varepsilon}(v) \, d\,\Omega = \int_\Omega v^\top F \, d\,\Omega + \int_\Gamma v^\top \widehat{\sigma_n} \, d\,S, \tag{2-15}$$

where

$$\widehat{\sigma}_n = \widehat{\nabla}_n^\top \widehat{\sigma}, \qquad \widehat{\nabla}_n^\top = \begin{bmatrix} n_x & 0 & n_y \\ 0 & n_y & n_x \end{bmatrix},$$

and n_x, n_y are the normal directions in x and y respectively. The elasticity problem in two dimensions contain two unknown differential equations in every point u_x and u_y, these are approximated in most cases by a linear combination of basis functions for the two components. If we are taking the same partition as in Ω for the minimum compliance design in two dimensions and define

$$P^1(\tau^h) = \left\{ v : \Omega \to \mathbb{R} \;\middle|\; \begin{array}{ll} v & \text{continuous function in } \Omega \\ v|_{Q_i} & \text{is a first degree polynomial function} \end{array} \right\}.$$

We can write the solution in this form:

$$u \approx u^h = \begin{bmatrix} \displaystyle\sum_{i=1}^{n} \varphi_{2i-1}\alpha_{2i-1} \\ \\ \displaystyle\sum_{i=1}^{n} \varphi_{2i}\alpha_{2i} \end{bmatrix}, \tag{2-16}$$

where φ contains the basis functions and the parameters in α are nodal displacements. In this mesh we define two basis functions, see more in [1]. The Galerkin's formulation is

$$\sum_{i\in I_\Omega}\int_\Omega C\left(\alpha_i\varepsilon(\varphi_i)\right)\varepsilon\varphi_j = \int_\Omega f\varphi_j - \sum_{l\in\partial\Omega}\int_\Omega C\left(\beta_l\varepsilon(\varphi_l)\right)\varepsilon(\varphi_j).$$

Define the following matrices and vectors,

$$a_{Eij} = \int_\Omega C\ \left(\varepsilon(\varphi_i)\right)\varepsilon(\varphi_j),$$

$$b_j = \int_\Omega f\varphi_j - \int_\Omega C\left(\beta_l\varepsilon(\varphi_l)\right)\varepsilon(\varphi)_j,$$

we can write this as a linear system

$$\mathbf{A_E}\vec{\alpha} = \overrightarrow{b_E} \tag{2-17}$$

where $A_{Eij} = a(\varphi_i, \varphi_j)$, with $i, j = 1, \ldots, k$. And $b_{Ej} = l(\varphi_j)$ for $j = 1, \ldots, k$.

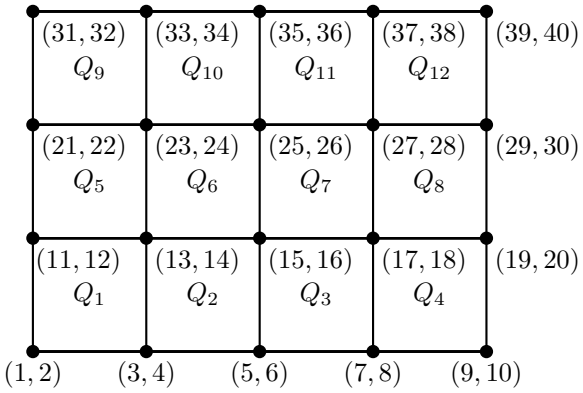

Figure **2-4**: Mesh over Ω for the elasticity problem, each node has two degrees of freedom (dof). Even labels represents horizontal dof while odd labels represent vertical dof.

2.4 Numerical experiments for the elasticity equation

In this section, we show some experiments for the elasticity problem described in (2-17) with different coefficients κ where

$$C_{ij} = \kappa C^0_{ij}. \tag{2-18}$$

And we use a tolerance of 1×10^{-6} for a 100×100 mesh and up to 2000 iterations in the *conjugate gradient method without preconditioning*. The goal is to demonstrate the

performance of the CG iterative method and to show its dependence of the contrast in the PDE coefficients.

Coefficient without channels that reach the domain border

The first coefficient in Figure **2-5**, we represent a material whit high stiffness in the middle of the domain. The high stiffness area is the black circle in the domain and the three different forcing terms in Figure **2-6** are applied in the high stiffness region.

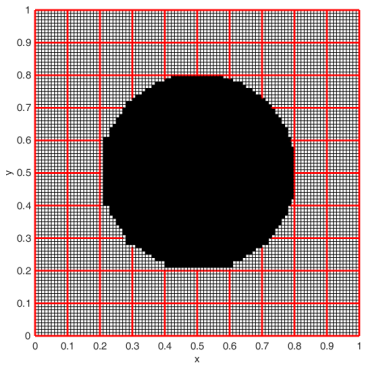

Figure **2-5**: Coefficient I, the high-stiffness channels reach the boundary.

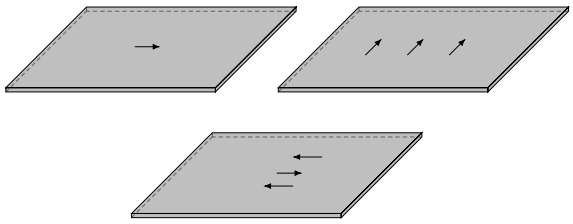

Figure **2-6**: Forcing terms applied to the circle shaped coefficient in figure **2-5**.

For different contrast values of the coefficient we solve the elasticity problem using the conjugate gradient without preconditioners and we get next results in table **2-3**.

	Forcing term A		Forcing term B		Forcing term C	
Coefficient	Iterations	Spectral condition	Iterations	Spectral condition	Iterations	Spectral condition
1	233	3.2×10^3	276	3.2×10^3	220	3.2×10^3
1×10^{-2}	1983	2.6×10^5	2000	2.6×10^5	2000	2.6×10^5
1×10^{-4}	2000	2.4×10^7	2000	2.4×10^7	2000	2.4×10^7
1×10^{-2}	2000	1.5×10^9	2000	1.5×10^9	2000	1.5×10^9

Table **2-3**: Elasticity problem using coefficient I defined in Figure **2-5**.

We observe large iteration number and the conjugate gradient fails to converge before 2000 iterations. We also observe that the number of iterations increase with the contrast.

Coefficient with the high stiffness channels reach the boundary

In this case, we take the coefficient in Figure **2-7**. The coefficient has three high stiffness channels over the domain, and has two channels reach the boundary domain. For this coefficient we apply the forces in Figure **2-8**.

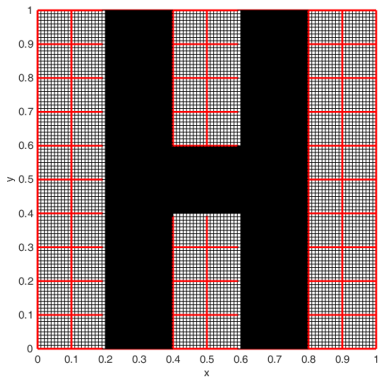

Figure **2-7**: Coefficient II, the high-stiffness channels reach the boundary.

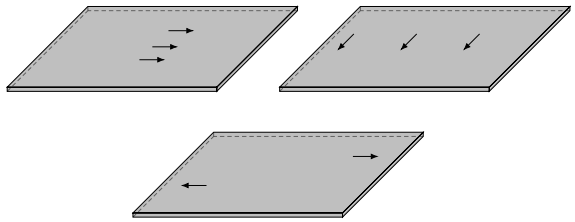

Figure **2-8**: Forcing terms applied to the H shaped coefficient II.

And, we solve the elasticity equation using the conjugate gradient method without preconditioners with the coefficient in Figure **2-7** and we get the next results in Table **2-4**.

	Forcing term A		Forcing term B		Forcing term C	
Coefficient	Iterations	Spectral condition	Iterations	Spectral condition	Iterations	Spectral condition
1	235	3.2×10^3	276	3.2×10^3	295	3.2×10^3
1×10^{-2}	1218	5.8×10^4	1212	4.7×10^4	1313	4.8×10^4
1×10^{-4}	2000	1.6×10^6	2000	2.8×10^6	2000	1.7×10^6
1×10^{-6}	2000	5.6×10^7	2000	6.3×10^7	2000	4.9×10^7

Table **2-4**: Elasticity problem without using coefficient II defined in Figure **2-7**.

We also observe in Table **2-4** large iteration counts as before and larger number of iterations when the contrast increase.

High contrast coefficient

In the last example we get a high contrast coefficient with high stiffness channels are connected over all the domain see in Figure **2-9**, and we apply two different forces over the domain, see in Figure **2-10**.

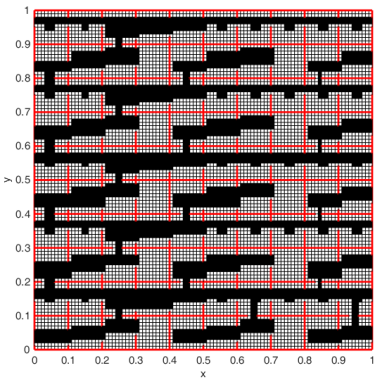

Figure **2-9**: Coefficient III, the high-stiffness channels reach the boundary.

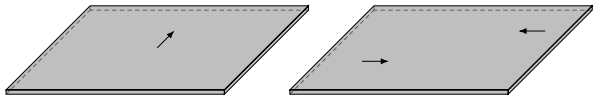

Figure **2-10**: Forcing terms applied to the coefficient III.

Solving the elasticity problem using the conjugate gradient without preconditioners and the high contrast coefficient in Figure **2-9** and we have the results in Table **2-5**. We observe similar results than before.

	Forcing term A		Forcing term B	
Coefficient	Iterations	Spectral condition	Iterations	Spectral condition
1	292	3.2×10^3	293	3.2×10^3
1×10^{-2}	1662	1.2×10^5	1583	1.2×10^5
1×10^{-4}	2000	8.6×10^5	2000	1.2×10^6
1×10^{-6}	2000	4.5×10^6	2000	4×10^6

Table **2-5**: Elasticity problem without preconditioner using coefficient III defined in Figure **2-9**.

The coefficient $\kappa_{ij}(x) = \kappa(x)\delta_{ij}$ represents the stiffness of the media Ω. We focus on two-levels overlapping domain decomposition and use local spectral information in constructing "minimal" dimensional coarse spaces (MDCS) within this setting. After some review on constructing MDCS and their use in overlapping domain decomposition preconditioners, we present an approach, which uses MDCS to minimize the condition number to a condition number closer to 1, see more in [17, 10, 16, 12].

We assume that there exists $\kappa_{\min}$ and $\kappa_{\max}$ with $0 < \kappa_{\min} \leq \kappa(x) \leq \kappa_{\max}$ for all $x \in \Omega$. The coefficient κ has a multiscale structure (significant local variations of κ occur across Ω at different scales). We regard that the coefficient κ is a high-contrast coefficient (the constrast is $\eta = \kappa_{\max}/\kappa_{\min}$). We consider that η is large compared to the coarse-grid size, see more in [17].

It is well known that performance of numerical methods for high-contrast multiscale problems depend on η and local variations of κ across Ω. For finite element methods, the condition to

obtain good approximation results is that the finite element mesh has to be fine enough to resolve the variations of the coefficient κ. For this reasons, finite element approximation leads to the solution of very large ill-conditioned problems (with the condition number scaling with h^{-2} and η). Therefore, the performance of solvers depends on η and local variations of κ across Ω, this was seen in [17, 14, 13, 6].
Let $\mathcal{T}^h$ be a triangulation of the domain Ω, where h is the size of a typical element. We consider only the case of discretization by the classical finite element method $V = P_1(\mathcal{T}^h)$ of piecewise (bi)linear functions. Other discretizations can also be considered. The application of the finite element discretization leads to the solution of a very large ill-conditioned system 2-17 where A_E is roughly of size h^{-2} and the condition number of A_E scales with η and h^{-2}. In general, the main goal is to obtain an efficient good approximation of solution u. The two main solution strategies are:

- Choose h sufficiently small and implement an iterative method. It is important to implement a preconditioner M^{-1} to solve $M^{-1}Au = M^{-1}b$. Then, it is important to have the condition number of $M^{-1}A$ to be small and bounded independently of physical parameters, e.g., η and the multiscale structure of κ, see more in [13, 9, 11, 10, 6, 12, 7, 15, 17].

- Solve a smaller dimensional linear system ($\mathcal{T}^H$ with $H > h$) so that computations of solutions can be done efficiently[1].

  This usually involves the construction of a downscaling operator R_0 (from the coarse-scale to fine-scale $v_0 \mapsto v$) and an upscaling operator (from fine-scale to coarse-scale, $v \mapsto v_0$) (or similar operators). Using these operators, the linear system $Au = b$ becomes a coarse linear system $A_0u_0 = b_0$ so that R_0u_0 or functionals of it can be computed. The main goal of this approach it to obtain a sub-grid capturing such that $||u - R_0u_0||$ is small, see more in [17, 14, 18, 30, 5, 16, 8, 7].

  Here we focus on the first option and, based in the results in [37] and [17, 26]. We design and numerically test several preconditioners for the elasticity eqquation, see also in [26]. The main idea is to use two levels domain descomposition with generalized multiscale finite element space for the second level.

[1] The coarse mesh does not necessarily resolve all the variations of κ.

3 Multiscale Methods

In this chapter we briefly describe the multiscale method making special emphases on the generalized multiscale method, which is used in this work, for a detailed explanation see [15, 36, 16] and [17]. In the high contrast elasticity problem in the last example of the previous chapter, we represent mixed material like ground, metal alloys or fibers. The properties of these materials are difficult to be obtained in a coarse mesh, but solving this type of problems in a fine mesh has great computational cost and takes a long time, for this reason, we use the multiscale method.
We investigate how to use a multiscale method to solve the high contrast problem using spectral multiscale basis functions [11]. In the multiscale method, we have two partitions of a domain, in the first partition we define a fine mesh (with more elements) and on the other one a coarse mesh. We want to approximate the solution in the fine mesh by solving local problems in the coarse mesh that needs less computational cost.
Multiscale basis in the coarse mesh is constructed with the eigenvectors of the spectral problem in each subdomain of the coarse space. The local spectral problem strongly depends on the choice of an initial partition of the unity functions that includes the properties of the original problem. Next, we present the construction of the basis functions of the coarse space and its advantages.

3.1 Generalized Multiscale Method

Let $\Omega \subset \mathbb{R}^2$ a polygonal domain and $\mathcal{T}^H$ a the coarse grid partition, with H the size of the coarse grid.
We consider the partial differential equation,

$$\begin{cases} -\operatorname{div}(\sigma(u)) = F & \text{in } \Omega, \\ \sigma(u) = C\varepsilon(u) & \text{in } \Omega, \end{cases}$$

defined in equation 2-12, where σ is the stress tensor, ε is the strain tensor, C is the stiffness tensor u is the displacement and F the external force. In this case we assume the material to be isotropic and

$$C_{ij} = \kappa C^0_{ij}$$

where κ is the contrast of the material defined in 2-18 also we assume that $\kappa_{\min}$ and $\kappa_{\max}$ exist, and $\kappa_{\min} \leq \kappa \leq \kappa_{\max}$ for all $x \in \Omega$.

We take the variational formulation of the elasticity problem in two dimensions defined in 2-15 and define bilinear form,

$$a_E(u,v) = \int_\Omega (C\varepsilon(u)) : \varepsilon(v)\, dx \quad \text{for all } u, v \in V, \tag{3-1}$$

and the linear form,

$$l(v) = \int_\Omega F : v\, d\Omega + \int_\Gamma \sigma_n : v\, dS \quad \text{for all } u, v \in V. \tag{3-2}$$

Let $\mathcal{T}^h$ be a fine triangulation which is a refinement of $\mathcal{T}^H$ like in Figure **3-1**.

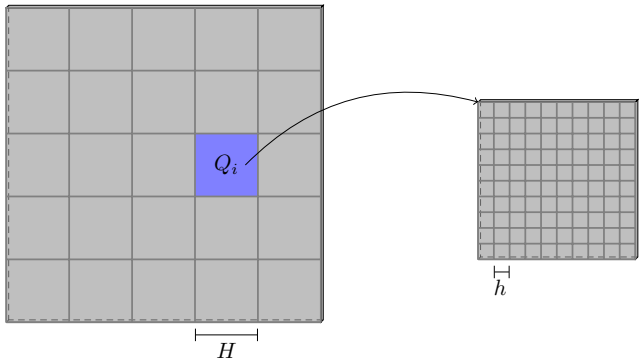

Figure **3-1**: Coarse grid and fine grid in square domain, where Q_i is an element the coarse space, H is the size of the coarse grid and h is the size of the fine grid.

We define $V^h(\Omega)$ the basis functions space that are piecewise linear continuous with respect to the fine triangulation $\mathcal{T}^h$.
The Galerkin formulation from [17] is: find $u \in V_0^h(\Omega)$ such that

$$a_E(u,v) = f(v),$$

and in the matrix form,

$$A_E u = b,$$

where $u, v \in V^h(\Omega)$,

$$u^\top A_E v = \int_\Omega (C\varepsilon(u)) : \varepsilon(v)\, dx,$$

and

$$v^\top b = \int_\Omega F : v\, dx.$$

We denote $\{y_i\}^{N_v}$ the vertices of the coarse mesh $\mathcal{T}^H$ and define the neighborhood of the node y_i by,

$$\omega_i = \cup\{Q_j \in \mathcal{T}^H; y_i \in Q_j\}, \tag{3-3}$$

and the neighborhood of the coarse element Q (see Figure **3-2**) by

$$\omega_Q = \cup\{\omega_j \in \mathcal{T}^H; y_j \in \bar{Q}\}. \tag{3-4}$$

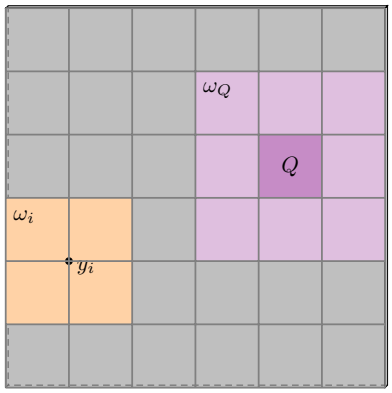

Figure **3-2**: The orange rectangle represent the neighborhood of node y_i called ω_i and the violet rectangle is the neighborhood of the coarse element Q.

In $\mathcal{T}^H$ we consider coarse functions $\{\phi_i\}_{i=1}^{N_Q}$ where N_Q is the number of coarse basis functions, see more in [11], and we consider a high contrast eigenvalue problem with a high-contrast coefficient defined in **2-9**.
For any $\omega_i \subset \Omega$, we define the Neumann matrix A^{Ω_i} as,

$$vA_E^{\omega_i} w = \int_\Omega (C\varepsilon(v)) : \varepsilon(w)\, dx \quad \text{for all } v, w \in V^h(\Omega),$$

and the mass matrix M^{ω_i} by

$$vM^{\omega_i} w = \int_\Omega (Cv)w \quad \text{for all } v, w \in V^h(\Omega).$$

The coarse basis function are obtained by solving the eigenvalue problem,

$$-\operatorname{div}(C(x)\varepsilon(u)) = \lambda\kappa(x)u, \qquad \text{for all } x \in \omega_i. \tag{3-5}$$

We use Neumann boundary condition on $\partial\omega_i \setminus \partial\Omega$ and Dirichlet condition on $\partial\omega_i \cap \partial\Omega$ it its not empty. In matrix form we have,

$$A_E^{\omega_i}\phi^{\omega_i} = \lambda M^{\omega_i}\phi^{\omega_i}, \tag{3-6}$$

and the eigenvalues and the eigenvectors are denoted as $\{\lambda_l^{\omega_i}\}$ and $\{\psi_l^{\omega_i}\}$ respectively and the eigenvalues are ordered as,

$$\lambda_1^{\omega_i} \leq \lambda_2^{\omega_i} \leq \lambda_3^{\omega_i} \leq \cdots \leq \lambda_j^{\omega_i} \leq \cdots$$

We construct a set of enriched multiscale basis functions given by $\chi_i\psi_\ell^{\omega_i}$ for the selected eigenvectors $\psi_\ell^{\omega_i}$. Using L_i to denote the number of basis functions from the coarse region ω_i, we then define the coarse GMsFEM space by

$$V_0 = \text{span}\{\phi_{i,\ell} = \chi_i\psi_\ell^{\omega_i}, \quad i = 1, \ldots, N_v, \quad \ell = 1, \ldots, L_i\}.$$

For a detailed construction and additional properties of the space V_0 see more in [9, 10, 11, 37]. Due to our numerical experiments we see that selection of the number of coarse basis in the elasticity case is complicated since the low modes of the spectrum doesn't show a clear behavior with the high-stiffness regions. The optimal number of low modes are to be related to the disconnected high-stiffness regions and to the RBM (rigid bod motions) of this regions. The space RBM of rigid bod modes on $\Omega \subset \mathbb{R}^d$ is defined for $d = 2$, by

$$\text{RBM}(\Omega)\left\{v \in [L^2(\Omega)]^2 : v = a + b\begin{pmatrix} -x_2 \\ x_1 \end{pmatrix}, a \in \mathbb{R}^2, b \in \mathbb{R}, x \in \Omega\right\}$$

As seen in Figure **3-3**, the basis elements depend on the number of high-stiffness regions, and per each region we add three basis, each one related to a RBM. In this work the selection of the coarse basis elements for the experiments is done in a manual way, i.e. we specify the quantity of basis elements based on the disconnected high-stiffness regions present in the specific overlap domain.

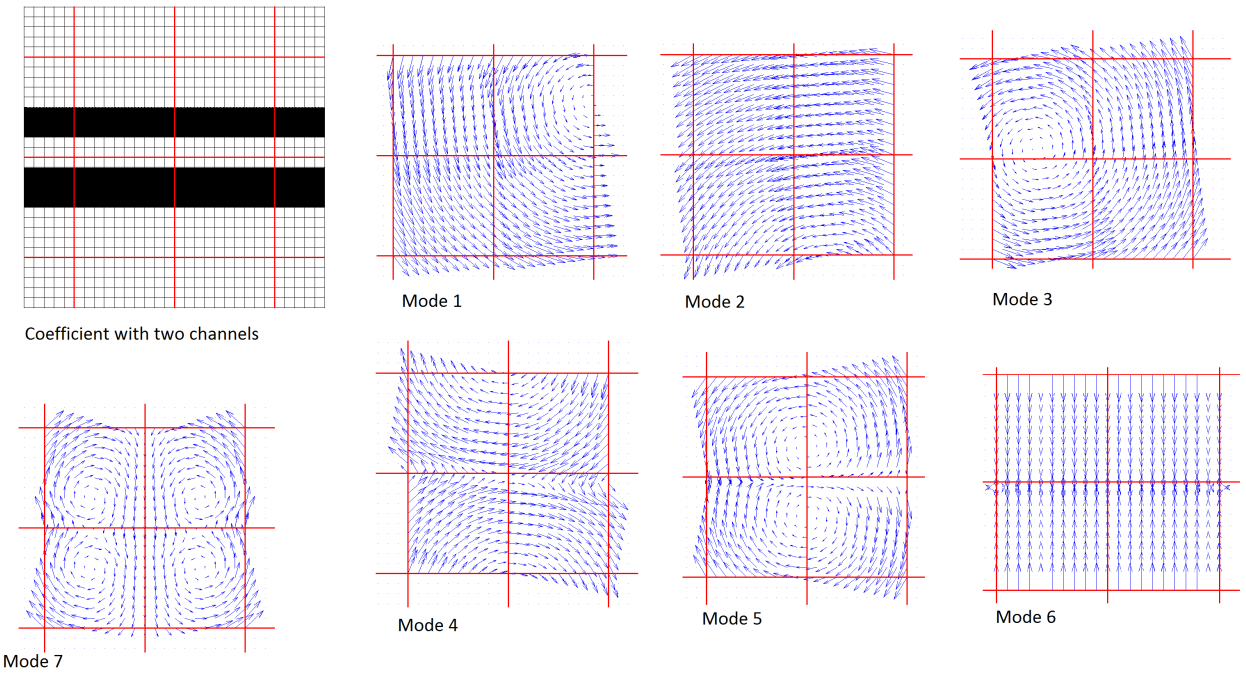

Figure **3-3**: Two disconnected high-stiffness regions and its contrast dependent modes. Three for each region corresponding to the RBM. The next mode is contrast independent.

We know that $\{\omega_l^{\omega_i}\}_{y_i \in \mathcal{T}^h}$ is a covering of Ω. Let $\{\chi_l\}_{i=1}^{N_v}$ be a partition of unity subordinated to the covering $\{\omega_l^{\omega_i}\}_{y_i \in \mathcal{T}^h}$ such that $\chi_i \in V^h(\Omega)$ and $|\nabla \chi_i| \leq \dfrac{1}{H}$ for $i = 1, \ldots N_v$.

$$\phi_{i,l} = \chi_i \psi_l^{\omega_i}, \tag{3-7}$$

where l_i is the number of eigenvalues, see more in [11].

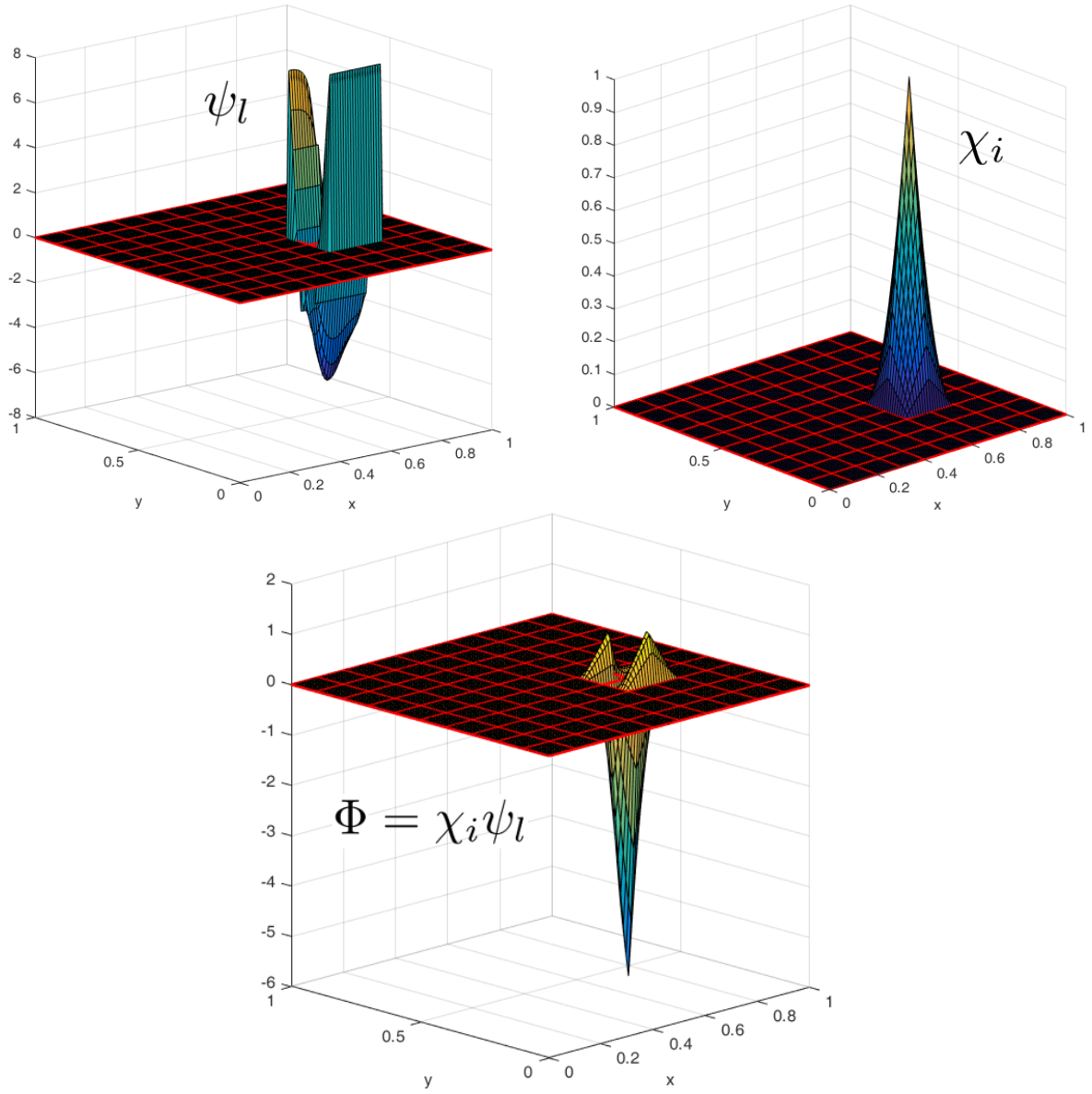

Figure **3-4**: Description of basis function construction for some element of the domain. We choose one eigenvector in the region and a linear function in the element and the last figure is the result of multiply the first ones.

For the elasticity problem the GMsFEM approximate the solution on a coarse grid as,

$$u_0 = \sum_i^{N_v} c_i \phi_i$$

where c_i are the unknown constant, and the new problem is

$$a_E(u_0, v) = F(v) \quad \text{for all } v \in \text{span}\{\phi_i\}_{i=1}^{N_c}.$$

Multiscale Finite Element Method also solve underlying fine-scale equation on the coarse grid. Given coarse scale basis function are determined by the coarse matrix

$$A_{E,0} = R_{E,0} A_E R_{E,0}^\top, \tag{3-8}$$

where

$$R_{E,0}^\top = [\phi_1 \quad \phi_2 \cdots \phi_{N_c}]. \tag{3-9}$$

Multiscale finite element solution is the finite element projection of fine-scale solution in V_0 as,

$$A_{E,0} u_0 = f_0, \tag{3-10}$$

where $f_0 = R_{E,0}^\top b$. Note the $R_{E,0} u_0$ is the approximation of the solution, see more details in [12, 17, 11, 16, 10, 9, 5, 6, 7, 8, 15].
In the next chapter we will use the multi-scale method to construct a two-level preconditioner for the elasticity equation. The multiscale method is the first level of the Schwarz additive preconditioner and we will also use it for the construction of low cost preconditioners.

4 Schwarz Domain Decomposition Method

In this chapter, we describe the two level overlapping Schwarz domain decomposition method for the heat and elasticity problems with different conductivity and stiffness coefficient, respectively. In the first part of the chapter, we present the main idea of the domain decomposition method for the Poisson problem and we construct the preconditioner with Schwarz additive method. After that, we study the abstract theory of the Schwarz Method, which is useful in the design and analysis of new and old iterative methods, and also gives the necessary requirements to convert linear systems of large and poorly conditioned algebraic equations into well-conditioned linear systems. Finally, we present some experiment with different coefficients for the isotropic elasticity problem and we compare the results with and without preconditioner.

4.1 Schwarz's method

A simple domain decomposition method was presented by H.A. Schwarz in 1870. Schwarz used an iterative algorithm to determine the existence of harmonic functions in non-smooth bounded regions.

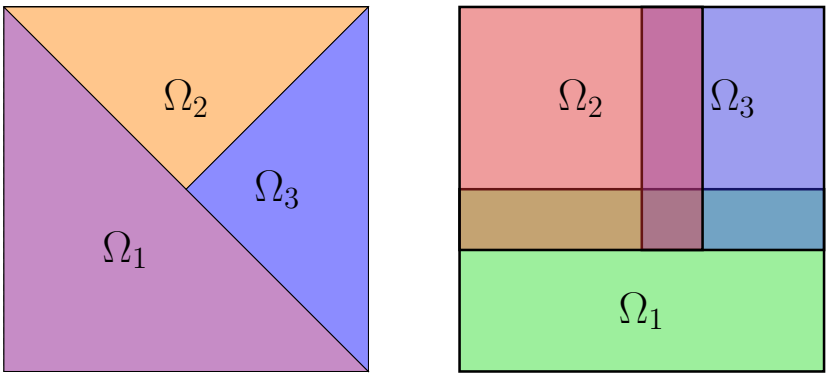

Figure **4-1**: Left figure: Domain divided into three non-overlapping subregions with the union of the original domain. Right figure: Domain divided into three overlapping subregions with the union of the original domain.

He constructed a region with the union of subregions see in Figure **4-1** and solve recursively the problem on each subregion. Schwarz proved that the iterative method converges on the norm of the maximum.
The idea of the recursive algorithm for a two-stage problem is,

- Solve the problem in a subregion.
- Solve the problem in the union of the other subregions using recursively the previous step.

Let us apply the Schwarz method in two regions for the Poisson problem (4-1) in a continuous region with Dirichlet boundary condition, using recursively the previous steps,

$$\begin{cases} -\Delta u &= f \quad \text{in } \Omega, \\ u &= 0 \quad \text{on } \partial\Omega. \end{cases} \tag{4-1}$$

We divide the domain Ω into two overlapping subregions Ω_1 and Ω_2 of the original region $\Omega = \Omega_1 \cup \Omega_2$, see more in [30].

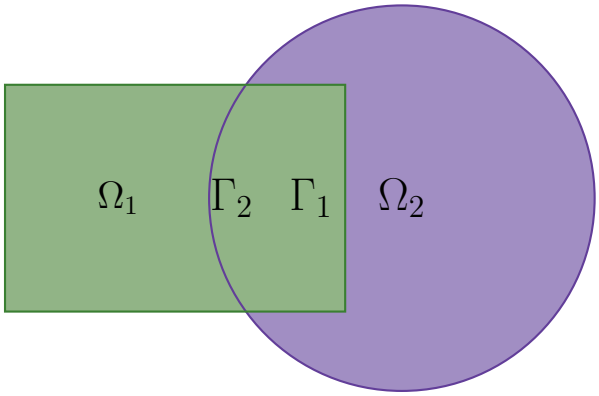

Figure **4-2**: Domain Ω divided in two domains Ω_1 and Ω_2, with borders Γ_1 and Γ_2 respectively.

Given an initial value u^0 that satisfies the boundary condition, the iteration u^{n+1} is determined by the previous iterations u^n, in two sequential steps whose solution approximates to the solution in both subdomains,

$$\begin{cases} -\Delta u^{n+1/2} = f & \text{in } \Omega_1, \\ u^{n+1/2} = u^n & \text{on } \partial\Omega_1, \\ u^{n+1/2} = u^n & \text{in } \Omega_2 - \overline{\Omega_1}. \end{cases} \tag{4-2}$$

In linear system 4-2 we describe the Poisson problem in the green rectangle in figure **4-2** and in the linear system 4-3 we analyze the blue circle region in Figure **4-2**.

$$\begin{cases} -\Delta u^{n+1} = f & \text{in } \Omega_2, \\ u^{n+1} = u^{n+1/2} & \text{on } \partial\Omega_2, \\ u^{n+1} = u^{n+1/2} & \text{in } \Omega_1 - \overline{\Omega_2}. \end{cases} \tag{4-3}$$

To analyze the problem we use the space V_0^1 and the bilinear form,

$$a(u,v) = \int_\Omega \nabla u \cdot \nabla v \, dx,$$

the Poisson problem defined in (4-1) can be written as

$$a(u,v) = \int_\Omega \nabla u \cdot \nabla v \, dx = \int_\Omega f v \, dx.$$

Choosing appropriate basis functions that spans V_0^1 and writing u as a linear combination of these functions, we can write this and similar problems in matrix formulation, as in (4-4). Now we can in order to use the finite element method

$$Au = b \tag{4-4}$$

where the matrix A is symmetric and positive definite.

Define V as the functions space defined over Ω, and V_i as the space of functions defined over Ω_i with $i = 1, 2$. We take the natural extension operators,

$$R_i^\top : V_i \to V, \qquad i = 1, 2.$$

The operator $R_i^\top$ take the local functions in V_i with zero in the border and extend them to Ω giving global functions in V, if we also define local bilinear forms,

$$a_i(u,v) = \int_{\Omega_i} \nabla u \cdot \nabla v \, dx,$$

we can write the Schwarz method as two orthogonal projections P_i with $i = 1, 2$, defined as,

$$P_i = R_i^\top \tilde{P}_i,$$

where $\tilde{P}_i : V \to V_i$ defined as

$$a_i(\tilde{P}_i u, v_i) = a(u, R_i^\top v_i), \qquad v_i \in V_i,$$

that means that if we solve the last equation in each subspace V_i we can find the solution of (4-1).

4.1.1 Block Jacobi Preconditioners

An important derivation of the Schwarz method is the Schwarz additive method, for which we are going to consider two-block Jacobi or the conjugate gradient. In the conjugate gradient method we are going to precondition A with a matrix A_J^{-1}, in the Poisson problem in 4-4 we have,

$$A_J^{-1} A u = A_J^{-1} b, \tag{4-5}$$

where the matrix A_J is the direct sum of the blocks of the diagonal of A. Each block of the matrix A_J corresponds to a set of degrees of freedom that define a subspace V_i, and the space V can be written as the direct sum of the subspaces V_i for $i = 1, 2$,

$$V = R_1^\top V_1 \oplus R_2^\top V_2,$$

where $R_i^\top$ are natural extension operators,

$$R_i^\top : V_i \to V, \qquad i = 1, 2,$$

and $R_i^\top$ take the set of degrees of freedom of V_i and extend them with zeros to the domain Ω. If we take A in V_i we denote it as A_i, the preconditioner A_J^{-1} can be written as,

$$A_J^{-1} = \begin{pmatrix} A_1^{-1} & 0 \\ 0 & 0 \end{pmatrix} + \begin{pmatrix} 0 & 0 \\ 0 & A_2^{-1} \end{pmatrix} = \begin{pmatrix} A_1 & 0 \\ 0 & A_2 \end{pmatrix}^{-1}$$

To write the compact form A_J of A, we proceed by eliminating the couplings between spaces V_i. As the coupling between the two spaces is smaller then the preconditioner is better, see more in [30].
To write more compactly A_J we write the operator,

$$R_i : V \to V_i, \qquad i = 1, 2,$$

where R_i is the adjoint operator of $R_i^\top$ with respect to the Euclidean scalar product. We know that R_i takes a vector with the complete set of degrees of freedom and extracts the degrees of freedom which corresponds to the subspace V_i which yields,

$$A_i = R_i A R_i^\top, \qquad i = 1, 2,$$

and,

$$A_J^{-1} = R_1^\top A_1^{-1} R_1 + R_2^\top A_2^{-1} R_2.$$

To connect the Schwarz method we introduce the additive projection operator:

$$P_{ad} = A_J^{-1} A,$$

which we can write using projections as,

$$P_i : R_i^\top A_i^{-1} R_i A : V \to V, \qquad i = 1, 2,$$

and

$$P_{ad} = P_1 + P_2.$$

Then P_{ad} is the sum of orthogonal projections in the internal product generated by the bilinear form $a(\cdot, \cdot)$ and is upper bounded. And the Poisson problem 4-4 can be written as the preconditioned system,

$$P_{ad} u = A_J^{-1} b.$$

4.2 Abstract Theory of Schwarz Methods

In the last section, we describe Schwarz domain decomposition with the Poisson problem but is but it is necessary to analyze the general case of the additive Schwarz method. In this section, we present some theorems and important assumptions that show the importance of the application .solving problems.

Consider a finite dimensional Hilbert space V, and the symmetric and positive definite bilinear form,

$$\begin{aligned} a(\cdot,\cdot) :& V \times V \to \mathbb{R} \\ & (u,v) \to a(u,v). \end{aligned}$$

Given $f \in V'$, we consider the problem of finding $u \in V$ such that,

$$a(u,v) = f(v), \qquad \text{for all } v \in V. \tag{4-6}$$

Given a basis of V, we can represent $u \in V$ uniquely by its degrees of freedom, like the linear functional $f \in V'$ which corresponds to a load vector.
We define A is the stiffness matrix associated with the bilinear form $a(\cdot,\cdot)$ in the problem (4-6) and b is the vector associated with the linear form f, we obtain the following linear system,

$$Au = b,$$

with A symmetric and positive definite.
We also consider a family of subspaces V_i with $i = 1, 2, \ldots, N$ and we assume that there exists interpolation operators $R_i^\top : V_i \to V$, called ***extension operator.*** The extension operator $R_i^\top$ extends the elements of subspace V_i into elements of space V.
Assuming that the space V admits the following decomposition

$$V = R_0^\top V_0 + \sum_{i=1}^{N} R_i^\top V_i, \tag{4-7}$$

this decomposition is not necessarily the direct sum of subspaces of V and in some cases the representation of V in function of V_i is not unique and also V_i is not always a subspace of V and the subspace V_0 represent the coarse space of multi-scale approach presented in the previous chapter.

In the subspaces V_i, we introduce the bilinear form associated to the subspaces V_i,

$$a_i(\cdot,\cdot) : V_i \times V_i \to \mathbb{R}, \quad \text{for all } i = 0, 1, \ldots, N,$$

defined as,

$$a_i(u_i, v_i) = a\left(R_i^\top u_i, R_i^\top v_i\right), \qquad u_i, v_i \in V_i.$$

The stiffness matrix associated to $a_i(\cdot,\cdot)$ is $A_i : V_i \to V_i$ defined as,

$$A_i = R_i A R_i^\top.$$

If we resolve

$$A_i u_i = b_i, \qquad u_i, v_i \in V_i,$$

and we obtain the projection in the subspace V_i for $i = 1, \ldots, N$.
We define the Schwarz operator in terms of the ***projection operators***,

$$P_i = R_i^\top \tilde{P}_i : H \to R_i V_i \subset V, \qquad i = 0, 1, \ldots, N, \tag{4-8}$$

where $\tilde{P}_i : V \to V_i$, is defined as:

$$a_i(\tilde{P}_i u, v_i) = a(u, R_i^\top v_i), \qquad v_i \in V_i, \tag{4-9}$$

with $\tilde{P}_i$ is well defined since the local bilinear forms are coercive and in case of exact solvers (see more in [30]),

$$a(P_i u, R_i^\top v_i) = a(u, R_i^\top v_i) \qquad v_i \in V_i \tag{4-10}$$

Lemma 1. The Schwarz operator P_i [30, p.36] can be written as,

$$P_i = R_i^\top A_i^{-1} R_i A, \qquad 0 \le i \le N,$$

where $a(\cdot,\cdot)$ is a symmetric and definite positive bilinear form [30, p.35], R_i is the interpolation operator [30, p.36] and A is the stiffness matrix [30, p.36]. In addition, P_i is self-adjoint with respect to the scalar product induced by $a(\cdot,\cdot)$ and positive semi-definite. If moreover the local bilinear form is given by 4-10, then P_i is a projection, i.e.,

$$P_i^2 = P_i.$$

Proof. If we consider the matrix form of $\tilde{P}_i$ defined by (4-9),

$$v_i^\top A_i \tilde{P}_i u = (R_i^\top v_i)^\top A u, \quad \text{for all } u \in V \quad \text{y } v_i \in V_i,$$

therefore, applying the transpose on the right side of the previous equation we have:

$$v_i^\top A_i \tilde{P}_i u = v_i^\top R_i A u,$$

and the last expression is for all $u \in V$ and $v_i \in V_i$, we find:

$$A_i \tilde{P}_i = R_i A,$$

with the last expression the operator $\tilde{P}_i$ can be written as:

$$\tilde{P}_i = A_i^{-1} R_i A, \tag{4-11}$$

and $P_i = R_i^\top \tilde{P}_i$. We also get from expression 4-11,

$$P_i = R_i^\top A_i^{-1} R_i A, \quad \text{for } 0 \leq i \leq N. \tag{4-12}$$

Now, we prove that P_i is a self-adjoint operator with the expression (4-12). Take $u, v \in \mathcal{V}$ and,

$$a(P_i u, v) = a((R_i^\top A_i^{-1} R_i A)u, v),$$

if we take the right side of the last equation it can be written as,

$$\begin{aligned} a((R_i^\top A_i R_i A)u, v) &= v^\top A(R_i^\top A_i^{-1} R_i A u), \\ &= (R_i^\top A_i^{-1} R_i A v)^\top A u, \\ &= a(u, P_i v), \end{aligned}$$

and we have,

$$a(P_i u, v) = a(u, P_i v).$$

P_i being positive and semi-definite is a consequence of the coercivity of the local bilinear forms,

$$\begin{aligned} a(P_i u, u) &= u^\top A P_i u, \\ &= u^\top A R_i^\top A_i R_i A u, \\ &= v_i^\top A_i^{-1} v_i \geq 0. \end{aligned}$$

Now, we prove that $P_i^2 = P_i$. We have from (4-12) that,

$$P_i^2 = R_i^\top A_i^{-1} R_i A R_i^\top A_i^{-1} R_i A,$$

and $A_i = R_i A R_i^\top$ we have,

$$P_i^2 = R_i^\top A_i^{-1} A_i A_i^{-1} R_i A,$$

and simplifying the previous expression we get,

$$P_i^2 = R_i^\top A_i^{-1} R_i A = P_i,$$

therefore the operator P_i is self-adjoint.
A set of subspaces and local bilinear forms can define a number of different Schwarz operators. Each one is defined by polynomials of operators $\{P_i\}$ without the zero term and we can notice that:

$$P_i u = R_i^\top \tilde{P}_i u,$$

and u the solution of (4-6). □

If we defined the **additive operator** as,

$$P_{ad} = \sum_{i=0}^{N} P_i. \tag{4-13}$$

The explicit form of the additive preconditioner is,

$$P_{ad} = A_{ad}^{-1} A, \qquad A_{ad}^{-1} = \sum_{i=0}^{N} R_i^\top \tilde{A}_i^{-1} R_i. \tag{4-14}$$

For the additive operator we estimate the condition number of P_{ad},

$$\kappa(P_a d) = \frac{\lambda_{max}(P_{ad})}{\lambda_{min}(P_{ad})}.$$

To prove bounds for the additive Schwarz operator, is enough to make the next three assumptions.

Assumption 1 (Stable Decomposition)**.** *There exists a constant C_0, such that every $u \in V$ admit a decomposition,*

$$u = \sum_{i=0}^{N} R_i u_i, \qquad \{u_i \in V_i, 0 \le i \le N\},$$

that satisfies,

$$\sum_{i=0}^{N} a_i(u_i, u_i) \le C_0^2 a(u, u). \tag{4-15}$$

Assumption 2 (Strengthened Cauchy-Schwarz Inequalities)**.** *There exist constants $0 \le \epsilon_{ij} \le 1$, for $1 \le i, j \le N$, such that*

$$|a(R_i^\top u_i, R_j^\top u_j)| \le \epsilon_{ij} a(R_i^\top u_i, R_j^\top u_j)^{1/2} a(R_i^\top u_i, R_j^\top u_j)^{1/2} \tag{4-16}$$

for $u_i \in V_i$ and $u_j \in V_j$. We denote the spectral radius of $\mathcal{E} = \{\epsilon_{ij}\}$ by $\rho(\mathcal{E})$.

Assumption 3 (Local Stability)**.** *There exist $\omega > 0$, such that,*

$$a(R_i^\top u_i, R_i^\top u_i) \le \omega a_i(u_i, u_i), \qquad u_i \in \text{range}(\tilde{P}_i) \subset V_i, \qquad 0 \le i \le N. \tag{4-17}$$

Lemma 2. Assuming the stable decomposition. Then,

$$a(P_{ad} u, u) \ge C_0^{-2} a(u, u), \qquad u \in V, \tag{4-18}$$

and consequently P_{ad} defined in [30, p.37] is invertible. In addition,

$$a(P_{ad}^{-1} u, u) = \min_{u_i \in V_i} \sum_{u = \sum R_i^\top u_i}^{N} a_i(u_i, u_i).$$

Proof. Applying u decomposition, we get,

$$a(u,u) = a\left(u, \sum_{i=0}^{N} R_i^\top u_i\right),$$

and given that $a(\cdot,\cdot)$ is a linear operator,

$$a(u,u) = \sum_{i=0}^{N} a(u, R_i^\top u_i).$$

If we express in terms of the space V_i, then by definition (4-9),

$$a(u,u) = \sum_{i=0}^{N} a_i(P_i u, u_i),$$

and using the Cauchy-Schwarz inequality in the last expression we have:

$$a(u,u) \leq \left(\sum_{i=0}^{N} a_i(\tilde{P}_i u, \tilde{P}_i u)\right)^{1/2} \left(\sum_{i=0}^{N} a_i(u_i, u_i)\right)^{1/2},$$

and using the stable decomposition yields,

$$a(u,u) \leq \left(\sum_{i=0}^{N} a_i(\tilde{P}_i u, \tilde{P}_i u)\right)^{1/2} \left(C_0^2 a(u,u)\right)^{1/2}.$$

Now we apply the Cauchy-Schwarz inequality in V_i and since the local bilinear forms are symmetric and positive definite we get:

$$a(u,u)^{1/2} \leq C_0 \left(\sum_{i=0}^{N} a_i(\tilde{P}_i u, \tilde{P}_i u)\right)^{1/2},$$

squaring and projecting to the Hilbert space V with the definition (4-9) as:

$$a(u,u) \leq C_0^2 \left(\sum_{i=0}^{N} a(u, R_i^\top \tilde{P}_i u)\right),$$

since $a(\cdot,\cdot)$ is linear,

$$a(u,u) \leq C_0^2 a\left(u, \sum_{i=0}^{N} R_i^\top \tilde{P}_i u\right),$$

and using the equivalence of P_i of the equation (4-12),

$$a(u,u) \leq C_0^2 a\left(u, \sum_{i=0}^{N} P_i u\right).$$

By definition of P_{ad} we have that,

$$a(u,u) \leq C_0^2 a\left(u, P_{ad}u\right),$$

this completes the proof of Lemma (4-18) and also yields that P_{ad} is invertible.

For the second part of the lemma, we find the $u \in V$ decomposition, as:

$$u_i = \tilde{P}_i P_{ad}^{-1} u \qquad o \leq i \leq N. \tag{4-19}$$

and

$$u = \sum_{i=0}^{N} R_i^{\top} u_i.$$

If we take the decomposition:

$$\sum_{i=0}^{N} a_i(u_i,u_i) = \sum_{i=0}^{N} a_i(\tilde{P}_i P_{ad}^{-1}u, \tilde{P}_i P_{ad}^{-1}u),$$

projecting in V with (4-9) we get that

$$\sum_{i=0}^{N} a_i(u_i,u_i) = \sum_{i=0}^{N} a(P_{ad}^{-1}u, R_i^{\top}\tilde{P}_i P_{ad}^{-1}u),$$

and since $a(\cdot,\cdot)$ is a bilinear form, we have:

$$\sum_{i=0}^{N} a_i(u_i,u_i) = a\left(P_{ad}^{-1}u, \sum_{i=0}^{N} R_i^{\top}\tilde{P}_i P_{ad}^{-1}u\right),$$

for the u decomposition yields,

$$\sum_{i=0}^{N} a_i(u_i,u_i) = a\left(P_{ad}^{-1}u, u\right).$$

The equation (4.2) is true for any decomposition of the form $u = \sum_{i=0}^{N} R_i^{\top} u$, and it can written as,

$$a(P_{ad}^{-1}u, u) = \sum_{i=0}^{N} a(P_{ad}^{-1}u, R_i^{\top}u_i),$$

projecting on the subspace V_i with (4-9),

$$a(P_{ad}^{-1}u, u) = \sum_{i=0}^{N} a_i(\tilde{P}_i P_{ad}^{-1}u, u_i),$$

by the inequality of Cauchy-Schwarz we have,

$$a(P_{ad}^{-1}u,u) \leq \left(\sum_{i=0}^{N} a_i(\tilde{P}_i P_{ad}^{-1}u, \tilde{P}_i P_{ad}^{-1}u)\right)^{1/2} \left(\sum_{i=0}^{N} a_i(u_i,u_i)\right)^{1/2},$$

and in the space V, we can write it as:

$$a(P_{ad}^{-1}u,u) \leq \left(\sum_{i=0}^{N} a(P_{ad}^{-1}u, R_i^{\top}\tilde{P}_i P_{ad}^{-1}u)\right)^{1/2} \left(\sum_{i=0}^{N} a_i(u_i,u_i)\right)^{1/2},$$

regard the decomposition (4.2) in the last expression and we get,

$$a(P_{ad}^{-1}u,u) \leq \left(\sum_{i=0}^{N} a(P_{ad}^{-1}u,u)\right)^{1/2} \left(\sum_{i=0}^{N} a_i(u_i,u_i)\right)^{1/2},$$

and since $a(\cdot,\cdot)$ is a bilinear and definite positive form, it yields that,

$$a(P_{ad}^{-1}u,u)^{1/2} \leq \left(\sum_{i=0}^{N} a_i(u_i,u_i)\right)^{1/2},$$

And if we take the minimum on the decomposition (4.2) in the last inequality we have,

$$a(P_{ad}^{-1}u,u) = \min_{u_i \in V_i \; u=\sum R_i^{\top} u_i} \sum_{i=0}^{N} a_i(u_i,u_i).$$

□

Lemma 3. Assuming the local stability and the inequalities of Cauchy-Schwarz, then for $i = 0,\ldots,N$ we have that,

$$||P_i||_a \leq \omega.$$

In addition,

$$a(P_{ad}u,u) \geq \omega(\rho(\mathcal{E})+1)a(u,u),$$

where $\rho(\mathcal{E})$ is the spectral radius.

Proof. By definition,

$$a(P_i u, P_i u) = a(R_i^{\top}\tilde{P}_i u, R_i^{\top}\tilde{P}_i u),$$

using local stability defined in (4-17) on the right side of the previous expression, we get

$$a(P_i u, P_i u) \leq \omega a_i(\tilde{P}_i u, \tilde{P}_i u),$$

applying (4-9) yields,

$$a(P_i u, P_i u) \leq \omega a(u, R_i^{\top}\tilde{P}_i u),$$

by the definition of P_i we have,

$$a(P_i u, P_i u) \leq \omega a(u, P_i u), \tag{4-20}$$

and consequently applying Cauchy Schwarz, we have,

$$a(P_i u, P_i u) \leq \omega a(u, u)^{1/2} a(P_i u, P_i u)^{1/2},$$

squaring and simplifying terms we get,

$$a(P_i u, P_i u) \leq \omega^2 a(u, u).$$

For the second inequality of the lemma, we consider the operator

$$\widehat{P} = \sum_{i=1}^{N} P_i \tag{4-21}$$

note the operator $\widehat{P} = P_{ad} - P_0$ given that the strengthened Cauchy-Schwarz inequality works for V_i with $1 \leq i \leq N$, so

$$a(P_{ad} u, u) = a(P_0 u, u) + a(\widehat{P}, u), \tag{4-22}$$

Let us consider,

$$a(\widehat{P}u, \widehat{P}u) = a\left(\sum_{i=1}^{N} P_i u, \sum_{j=1}^{N} P_j u\right)$$

as $a(\cdot, \cdot)$ is the bilinear form, we get

$$a(\widehat{P}u, \widehat{P}u) = \sum_{i=1}^{N} \sum_{j=1}^{N} a\left(P_i u, P_j u\right)$$

and using the strengthened Cauchy-Schwarz inequalities,

$$a(\widehat{P}u, \widehat{P}u) \leq \sum_{i=1}^{N} \sum_{j=1}^{N} \varepsilon_{ij} a\left(P_i u, P_i u\right)^{1/2} a(P_j u, P_j u)^{1/2}.$$

Using (4-20) the last expression yielding,

$$a(\widehat{P}u, \widehat{P}u) \leq \sum_{i=1}^{N} \sum_{j=1}^{N} \varepsilon_{ij} \omega^{1/2} a\left(u, P_i u\right)^{1/2} \omega^{1/2} a(u, P_j u)^{1/2}.$$

by the symmetry of $\mathcal{E}$, and that therefore in l_2 norm is equal to its the spectral radius, we can write

$$a(\widehat{P}u, \widehat{P}u) \leq \sum_{i=1}^{N} \omega \rho(\mathcal{E}) a\left(u, P_i u\right),$$

and using the definition of $\widehat{P}$, we get

$$a(\widehat{P}u, \widehat{P}u) \leq \omega\rho(\mathcal{E})a\left(u, \widehat{P}u\right),$$

finally we have,

$$a(\widehat{P}u, \widehat{P}u) \leq \omega\rho(\mathcal{E})a\,(u,u)^{1/2}\,a(\widehat{P}u, \widehat{P}u)^{1/2}.$$

In the other hand, using Cauchy-Schwarz inequality yields,

$$a(\widehat{P}u, u) \leq a(\widehat{P}u, \widehat{P}u)^{1/2} a(u,u)^{1/2},$$

then

$$a(\widehat{P}u, u) \leq \omega\rho(\mathcal{E})a(u,u)^{1/2},$$

and using the bound for $||P_0||_a \leq \omega$, we find

$$\begin{aligned} a(P_{ad}u, u) &= a(P_0u, u) + a(\widehat{P}u, u), \\ &\leq \omega\, a(u,u) + \omega\rho(\mathcal{E})a(u,u), \end{aligned}$$

and we finally get

$$a(P_{ad}u, u) \leq \omega(\rho(\mathcal{E}) + 1)a(u,u).$$

□

Theorem 1 (Addive operator's condition number)**.** *Let stable descomposition, local stability and strengthened Cauchy-Schwarz inequalities be satisfied. Then the condition number of the additive Schwarz operator satisfies*

$$\kappa(P_{ad}) \leq C_0^2\omega(\rho(\mathcal{E}) + 1).$$

Proof. We estimate the condition number of P_{ad} as

$$\kappa(P_{ad}) = \frac{\lambda_{\max}(P_{ad})}{\lambda_{\min}(P_{ad})}, \tag{4-23}$$

where

$$\lambda_{\max} = \sup_{u\in V} \frac{a(P_{ad}u, u)}{a(u,u)} \qquad \text{and} \qquad \lambda_{\min} = \inf_{u\in V} \frac{a(P_{ad}u, u)}{a(u,u)},$$

see more in [30]. Using previous lemmas we have

$$a(P_{ad}u, u) \geq C_0^{-2} a(u,u) \qquad \text{and} \qquad a(P_{ad}u, u) \leq \omega(\rho(\mathcal{E}) + 1)a(u,u).$$

Hence,

$$\begin{aligned} \sup_{u\in V} \frac{a(P_{ad}u, u)}{a(u,u)} &\leq \frac{\omega(\rho(\mathcal{E}) + 1)a(u,u)}{a(u,u)} \\ &= \omega(\rho(\mathcal{E}) + 1), \end{aligned}$$

and

$$\begin{aligned}\inf_{u\in V}\frac{a(P_{ad}u,u)}{a(u,u)} &\leq \frac{C_0^{-2}a(u,u)}{a(u,u)}\\ &= C_0^{-2}.\end{aligned}$$

We get

$$\kappa(P_{ad})=\frac{\sup\limits_{u\in V}\dfrac{a(P_{ad}u,u)}{a(u,u)}}{\inf\limits_{u\in V}\dfrac{a(P_{ad}u,u)}{a(u,u)}}\leq C_0^2\omega(\rho(\mathcal{E})+1), \tag{4-24}$$

this complete the proof. □

In the next section we apply domain decomposition method in the heat and elasticity problems and we obtain the two level preconditioner for both equations.

4.3 Two level preconditioner for the heat equation

Let $H_0^1(\Omega)$ be the subspace of functions $v\in H^1(\Omega)$ with $v|_{\partial\Omega}=0$. Note that if we define

$$a(u,v)=\int_\Omega (K\nabla u)\nabla v,\ \text{and}\ \ l(v)=\int_\Omega fv,$$

we see that $a(u,v)$ is a bilinear form and $l(v)$ is a linear functional.
To obtain the Galerkin formulation of the problem we need to take $v\in V^h$ where V^h is a finite dimensional space. Here $h>0$ is a discretization parameter. We also need to choose a basis for V^h, say $\{\varphi_1,\varphi_2,\ldots,\varphi_k\}$ with k the dimension of V^h. We can approximate the temperature u with u_h over the domain using a linear combination of basis functions and write $u_h=\sum_{j=1}^k\alpha_j\varphi_j$, with α_j unknown coefficients. Within Galerkin's formulation, we should find $u_h\in V^h$ such that

$$\sum_{i\in I_\Omega}\int_\Omega K\ (\alpha_i\nabla\varphi_i)\,\nabla\varphi_j=\int_\Omega f\varphi_j-\sum_{l\in\partial\Omega}\int_\Omega K\,(\beta_l\nabla\varphi_l)\,\nabla\varphi_j.$$

And we can write this as a linear system

$$\mathbf{A}\vec{\alpha}=\vec{b} \tag{4-25}$$

where $A_{ij}=a(\varphi_i,\varphi_j)$, with $i,j=1,\ldots,k$. And $b_j=l(\varphi_j)$ for $j=1,\ldots,k$.
Now, we introduce a non-overlaping decomposition $\{\Omega_i\}_{i=1}^N$ in Ω that is,

$$\Omega=\bigcup_{i=1}^N\bar{\Omega}_i,$$
$$\Omega_i\cap\Omega_j=\emptyset\quad\text{for}\quad i\neq j$$

Construct an overlapping decomposition $\{\Omega_i'\}_{i=1}^N$ by adding a layer of width δ to each Ω_i and we have,

$$V^h(\Omega_i) = \left\{v^h \in V^h : supp(v^h) \leq \Omega_i'\right\}$$
$$V_0 = V_0^{ms},$$

where V_0^{ms} is the space in the multiscale method. We define the local sub-matrices of A corresponding the subdomains V_i by

$$A_i = R_i A R_i^\top,$$

where $R_i : V_i \to V$ is the restriction matrix and $R_i^\top : V \to V_i$ is the extension matrix. In the other hand, we take coarse triangulation Q^H of Ω' into coarse element, with $V_0^H \subset V_O^h$ coarse space.The function $\phi^H \in V_0^H$ omits a representation with respect to the fine scale basis.
In the coarse space, the stiffness matrix is given by

$$A_0 = R_0 A R_0^\top,$$

where $R_0 : V_0^H \to V_0^h$ is the restriction matrix in the coarse space to fine space and $R_0^\top$ is the extension matrix.
The additive Schwarz preconditioned is $M_H^{-1}A$ where the preconditioned matrix if defined by,

$$M_H^{-1} = M_{H,1}^{-1} + M_{H,2}^{-1}, \tag{4-26}$$

where the part corresponding to the first level is

$$M_{H,1}^{-1} r = \sum_{i=1}^{N} R_i A_i^{-1} R_i^\top r, \tag{4-27}$$

and the part corresponding to the second (or coarse) level is

$$M_{H,2}^{-1} r = R_0 A_0^{-1} R_0^\top r \tag{4-28}$$

where $A_0 = RAR^T$. Here the matrix R is a matrix where each column is a coarse basis function. Here the basis functions are of the form $\chi_i \psi_\ell$ where χ_i is a partition of unity function and ψ_ℓ are eigenvalues of a generalized eigenvalue problem.

4.4 Preconditioner for the elasticity equation

The elasticity problem, in two dimensions, defined in 2-13 contains two unknown differential equations in every point u_x and u_y, these are approximated in most cases by a linear combination of basis functions for the two components. We can write this as a linear system

$$\mathbf{A_E}\alpha = b_E \tag{4-29}$$

where $A_{Eij} = a(\varphi_i, \varphi_j)$, with $i, j = 1, \ldots, k$. And $b_{Ej} = l(\varphi_j)$ for $j = 1, \ldots, k$. Now, we introduce a non-overlaping decomposition $\{\Omega_i\}_{i=1}^N$ in Ω that is,

$$\Omega = \bigcup_{i=1}^{N} \bar{\Omega}_i,$$
$$\Omega_i \cap \Omega_j = \emptyset \quad \text{for} \quad i \neq j$$

Construct an overlapping decomposition $\{\Omega_i'\}_{i=1}^N$ by adding a layer of width δ to each Ω_i and we have,

$$V^h(\Omega_i) = \left\{ v^h \in V^h : supp(v^h) \leq \Omega_i' \right\}$$
$$V_0 = V_0^{ms},$$

where V_0^{ms} is the space in the multi-scale method. We define the local sub-matrices of A_E corresponding the subdomains V_i by

$$A_{E,i} = R_{E,i} A_E R_{E,i}^\top,$$

where $R_{E,i} : V_i \to V$ is the restriction matrix and $R_{E,i}^\top : V \to V_i$ is the extension matrix. In the other hand, we take coarse triangulation Q^H of Ω' into coarse element, with $V_0^H \subset V_0^h$ coarse space.The function $\phi^H \in V_0^H$ omits a representation with respect to the fine scale basis.
In the coarse space, the stiffness matrix is given by

$$A_{E,0} = R_{E,0} A_E R_{E,0}^\top,$$

where $R_{E,0} : V_0^H \to V_0^h$ is the restriction matrix in the coarse space to fine space and $R_0^\top$ is the extension matrix. The additive Schwarz preconditioner is $M_E^{-1} A_E$ where the preconditioned matrix if defined by,

$$M_E^{-1} = M_{E,1}^{-1} + M_{E,2}^{-1}, \tag{4-30}$$

where the part corresponding to the first level is

$$M_{E,1}^{-1} r = \sum_{i=1}^{N} R_{E,i} A_{E,i}^{-1} R_{E,i}^\top r, \tag{4-31}$$

and the part corresponding to the second (or coarse) level is

$$M_{E,2}^{-1} r = R_{E,0} A_{E,0}^{-1} R_{E,0}^\top r \tag{4-32}$$

where $A_{E,0} = R_E A_E R_E^T$. Here the matrix R_E is a matrix where each column is a coarse basis function. Here the basis functions are of the form $\chi_i \psi_\ell$ where χ_i is a partition of unity function and ψ_ℓ are eigenvalues of a generalized eigenvalue problem.

4.4.1 Experiments for the elasticity preconditioner

The next experiments we use the same coefficients used in previous chapter. And we take a tolerance of 1×10^{-6} and up to 2000 iterations in the *conjugate gradient method with preconditioning*. We use a 10×10 coarse mesh and inside each coarse-element we have a 10×10 fine-mesh.

Elasticity problem with coefficient I

For solve the elasticity problem with two level preconditioner, we take the coefficient in the Figure **2-5** and the vector forces in the Figure **2-6**, and we have the results in the Table **4-1** for the forces in Figure **2-6**.

	Forcing term A		Forcing term B		Forcing term C	
Coefficient	Iterations	Spectral condition	Iterations	Spectral condition	Iterations	Spectral condition
1	14	4.5	14	4.6	14	4.5
1×10^{-2}	16	5.3	16	5.3	16	5.3
1×10^{-4}	17	5.3	17	5.3	17	5.3
1×10^{-6}	17	5.3	17	5.3	18	5.3

Table **4-1**: Results of the elasticity equation with two level precondicioner using coefficient I defined in Figure **2-5**.

Elasticity problem with coefficient II

We regard the coefficient in Figure **2-7** and force vector in Figure **2-8**, and we get the results in table **4-2**.

	Forcing term A		Forcing term B		Forcing term C	
Coefficient	Iterations	Spectral condition	Iterations	Spectral condition	Iterations	Spectral condition
1	14	4.6	14	4.6	14	4.5
1×10^{-2}	16	5.3	15	5.2	16	5.1
1×10^{-4}	16	5.3	15	5.2	16	5.1
1×10^{-6}	16	5.3	15	5.2	16	5.1

Table **4-2**: Results of the elasticity equation with elasticity eigenvectors using coefficient II defined in Figure **2-7**.

Elasticity problem with coefficient III

In this example, we take the complex coefficient in the Figure **2-9** and the vector forces in Figure **2-10**. And we get the next results in Table **4-3**.

	Forcing term A			Forcing term B		
Coefficient	Iterations	Spectral condition	$\dim A_0$	Iterations	Spectral condition	$\dim A_0$
1	14	4.6	243	14	4.6	243
1×10^{-2}	29	16.7	387	26	16.0	387
1×10^{-4}	62	114.6	387	53	113.8	387
1×10^{-6}	61	257.2	387	44	140.6	387

Table **4-3**: Results of the elasticity equation with elasticity eigenvectors using coefficient III defined in Figure **2-9**.

Comparing the Tables **2-3**, **2-4** and **2-5** obtained by solving the elasticity problem without preconditioner in chapter 2, and Tables **4-1**, **4-2** and **4-3**, it can be noted that the spectral condition of the matrix improves when the preconditioner is applied. In addition, the number of iterations is considerably reduced when the preconditioner is applied to the elasticity equation. We also observe that the number of iterations (and estimated condition numbers) does not depend on the contrast as before. As showed in [17], here the use or several basis functions per node is of fundamental importance, as well as the fact that these basis functions are constructed using a local eigenvalue problem.

The table also shows the dimension of the coarse matrix has a maximum value of 387 for the high contrast coefficient, and although the values are better than those in Table **4-3**, the cost of calculating the eigenvectors for the coarse matrix is very high so we try to find a two levels preconditioner for the elasticity equation combining elasticity with heat.

5 Lower cost preconditioners for the elasticity equation

In this chapter we combine heat preconditioners in (4-27) and (4-28) studied in [37] with elasticity preconditioners in (4-31) and (4-32) to decrease the number of iterations of the elasticity problem with fewer computational cost since the heat problem is smaller than the elasticity problem.

The motivation to use the heat preconditioner is the master tesis [37] and in a work [20, 19]. In [37] the author shows the operation of the heat preconditioners to solve topological optimization problems we analyze the performance of the Schwarz two-levels preconditioners applied to the topology optimization problem for the heat equation. These preconditioners are built using a domain decomposition method and the generalized multiscale finite element method (GMsFEM) recently introduced. It is known that for a good performance of the preconditioner it is important the design of the basis functions. In this document, the calculation of multiscale basis functions uses the solution of carefully selected local eigenvalue problems as usual in the GMsFEM. We also propose the approximation of the local eigenvalues using a randomized algorithm to obtain an overall less expensive methodology, see in [26].

Finally, we show some results and advantages of each preconditioner, and we choose the one that reduces the computational cost and that decrease the number of iterations. With this preconditioner, we present other modifications to improve convergence.

5.1 High contrast Coefficients

For both problems, we take three different coefficients and different forcing vectors. In the heat problem, the coefficient represents the conductivity in the media and the force vector stand for a source of heat applied to the body. In the elasticity problem, the coefficient is the stiffness of the material and the force vector represent the external forces applied.
The coefficients represent the properties of the medium that we are going to analyze, in our case the three following coefficients are academic examples. We use the coefficient in previous chapter for the elasticity problem, and we apply the coefficient κ, in heat problem in the conductivity matrix,

$$K_{ij} = \kappa K^0_{ij}, \tag{5-1}$$

and in the elasticity problem as,

$$C_{ij} = \kappa C^0_{ij}. \tag{5-2}$$

- ***Coefficient without channels that reach the domain border*** The first coefficient in Figure **2-5**, we represent a material whit high conductivity (stiffness) in the middle of the domain. The high conductivity (stiffness) area is the black circle in the domain. This coefficient does not have high conductivity channels in the border of the domain and the three different forcing terms in Figure **2-6** are applied in the high stiffness region.

- ***Coefficient with the high stiffness reaching the boundary***
  We use the coefficient in Figure **2-7** in previous chapter for the elasticity problem. This coefficient is different from the previous one. It has two high conductivity channels that pass through the domain border and have three high conductivity channels. And we use the three forcing terms in Figure **2-8**.

- ***High-contrast coefficient*** The last coefficient in Figure **2-9** represent the complex material with high conductivity connected channels in the domain, and the Figure **2-10** has the forces in the high conductivity channels.

5.1.1 Block-diagonal one level preconditioner for the elasticity equation

In the first experiment, we apply the first level of heat preconditioner in the equation 4-27 within the elasticity problem.

$$\begin{bmatrix} M^{-1}_{H,1} & 0 \\ 0 & M^{-1}_{H,1} \end{bmatrix} A_E u_E = \begin{bmatrix} M^{-1}_{H,1} & 0 \\ 0 & M^{-1}_{H,1} \end{bmatrix} b_E.$$

Observe that here we use a block-diagonal preconditioner where in each block (that is, in each direction x and y) we use the one-level preconditioner constructed previously for the heat equation. If we solve the previous preconditioned elasticity problem for different contrast in the coefficient κ we obtain the results in Tables **5-1**, **5-2** and **5-3**.

- ***Coefficient without channels that reach the domain border***

	Forcing term A		Forcing term B		Forcing term C	
Coefficient	Iterations	Spectral condition	Iterations	Spectral condition	Iterations	Spectral condition
1	40	83	48	83	40	83
1×10^{-2}	92	4.3×10^3	93	4.3×10^3	94	4.3×10^3
1×10^{-4}	123	4.2×10^5	124	4.2×10^5	126	4.2×10^5
1×10^{-6}	159	4.2×10^7	159	4.2×10^7	160	4.2×10^7

Table **5-1**: Elasticity problem with a block-diagonal one level preconditioner using coefficient I defined in Figure **2-5** with load forces in Figure **2-6**.

- ***Coefficient with the high stiffness reach the boundary***

	Forcing term A		Forcing term B		Forcing term C	
Coefficient	Iterations	Spectral condition	Iterations	Spectral condition	Iterations	Spectral condition
1	42	83	48	83	51	83
1×10^{-2}	92	8.6×10^2	78	1.6×10^2	96	8.6×10^2
1×10^{-4}	96	1.1×10^3	97	1.1×10^3	98	1.1×10^3
1×10^{-6}	96	1.1×10^3	97	1.1×10^3	98	1.1×10^3

Table **5-2**: Elasticity problem with a block-diagonal one level preconditioner using coefficient II defined in Figure **2-7** and the load forces in Figure **2-8**.

- ***High-contrast coefficient***

	Forcing term A		Forcing term B	
Coefficient	Iterations	Spectral condition	Iterations	Spectral condition
1	42	83	42	83
1×10^{-2}	156	6.9×10^2	156	6.9×10^2
1×10^{-4}	611	8×10^3	611	8×10^3
1×10^{-6}	761	5.7×10^4	761	5.7×10^4

Table **5-3**: Elasticity problem with a block-diagonal one level preconditioner using coefficient III defined Figure **2-9** and the load forces in **2-10**.

Comparing the results in Tables **2-3**, **2-4** and **2-5** solving the elasticity problem without preconditioner with Tables **5-1**, **5-2** and **5-3** the number of iterations decreases when the preconditioner is applied but the spectral condition increases. Comparing with the results of the tables **4-1**, **4-2** and **4-3** the block-diagonal one level preconditioner does not give good results in the elasticity equation.

5.1.2 Block-diagonal two-level preconditioner for the elasticity equation

In this example we take the domain decomposition's matrix of the heat equation in the following form

$$\begin{bmatrix} M_H^{-1} & 0 \\ 0 & M_H^{-1} \end{bmatrix}.$$

That is, the block-diagonal preconditioner in equation 4-26 where in each block we employ the two-levels preconditioner constructed previously for the heat equation. Therefore, the

linear system for the elasticity problem is

$$\begin{bmatrix} M_H^{-1} & 0 \\ 0 & M_H^{-1} \end{bmatrix} A_E u_E = \begin{bmatrix} M_H^{-1} & 0 \\ 0 & M_H^{-1} \end{bmatrix} .b_E.$$

If we change the coefficient κ in the linear system we obtain the values for the solution in the Tables **5-4**, **5-5** and **5-6**.

- ***Coefficient without channels that reach the domain border***

	Forcing term A		Forcing term B		Forcing term C	
Coefficient	Iterations	Spectral condition	Iterations	Spectral condition	Iterations	Spectral condition
1	22	10	22	10	22	9.4
1×10^{-2}	38	3.5×10^2	39	3.5×10^2	38	3.5×10^2
1×10^{-4}	52	3.4×10^4	52	3.4×10^4	51	3.4×10^4
1×10^{-6}	67	3.4×10^6	67	3.4×10^6	66	3.4×10^6

Table **5-4**: Block-diagonal two-level preconditioner using coefficient I defined in Figure **2-5** and load forces in Figure **2-6**.

- ***Coefficient with the high stiffness reach the boundary***

	Forcing term A		Forcing term B		Forcing term C	
Coefficient	Iterations	Spectral condition	Iterations	Spectral condition	Iterations	Spectral condition
1	23	11	22	10	23	11
1×10^{-2}	42	51	38	49	41	51
1×10^{-4}	43	64	40	64	43	64
1×10^{-6}	4 3	64	40	64	43	64

Table **5-5**: Block-diagonal two-level preconditioner using coefficient II defined in Figure **2-7** and load forces in Figure **2-8**.

- ***High-contrast coefficient***

	Forcing term A		Forcing term B	
Coefficient	Iterations	Spectral condition	Iterations	Spectral condition
1	22	10	23	11
1×10^{-2}	89	1.5×10^2	78	1.5×10^2
1×10^{-4}	295	2.2×10^3	244	2.2×10^3
1×10^{-6}	345	1.5×10^4	266	7.5×10^3

Table **5-6**: Block-diagonal two-level preconditioner using coefficient III defined in Figure **2-9** and load forces in Figure **2-10**.

Comparing the results in Tables **4-1**, **4-2** and **4-3** solving the two level elasticity preconditioner with Tables **5-4**, **5-5** and **5-6**, in block diagonal two level preconditioner there are more iterations than in the preconditioner and also the spectral condition does not decrease.

5.1.3 Block-diagonal one level preconditioner with elasticity coarse projection in the coarse level

In this example we take the first level of the domain decomposition matrix of the heat problem in the equation 4-26 and we modify the coarse level of the preconditioner. That is,

$$M_E^{-1} = \begin{bmatrix} M_H^{-1} & 0 \\ 0 & M_H^{-1} \end{bmatrix} + \begin{bmatrix} R_0 \\ R_0 \end{bmatrix} A_{0,E}^{-1} \begin{bmatrix} R_0 \\ R_0 \end{bmatrix}^\top,$$

where

$$A_{0,E} = \begin{bmatrix} R_0 \\ R_0 \end{bmatrix} A_E \begin{bmatrix} R_0 \\ R_0 \end{bmatrix}^\top.$$

If we solve the elasticity problem using this preconditioner for different values of the contrast and forces, we obtain the results in Tables **5-7**, **5-8** and **5-9**.

- ***Coefficient without channels that reach the domain border***

	Forcing term A		Forcing term B		Forcing term C	
Coefficient	Iterations	Spectral condition	Iterations	Spectral condition	Iterations	Spectral condition
1	28	19	28	19	27	18
1×10^{-2}	36	28	37	28	35	28
1×10^{-4}	44	40	46	40	43	40
1×10^{-6}	54	52	55	52	52	52

Table **5-7**: Results of Block-diagonal one level preconditioner with elasticity coarse projection in the coarse level using coefficient I defined in Figure **2-5** and load forces in Figure **2-6**.

- ***Coefficient with the high stiffness reaching the boundary***

	Forcing term A		Forcing term B		Forcing term C	
Coefficient	Iterations	Spectral condition	Iterations	Spectral condition	Iterations	Spectral condition
1	29	21	28	19	29	21
1×10^{-2}	39	31	35	30	38	30
1×10^{-4}	40	31	36	31	38	31
1×10^{-6}	40	31	36	31	38	31

Table **5-8**: Results of Block-diagonal one level preconditioner with elasticity coarse projection in the coarse using coefficient II defined in Figure **2-7** and load forces in Figure **2-8**.

- ***High-contrast coefficient***

	Forcing term A		Forcing term B	
Coefficient	Iterations	Spectral condition	Iterations	Spectral condition
1	27	19	29	21
1×10^{-2}	96	2.6×10^2	86	2.4×10^2
1×10^{-4}	212	2.1×10^3	200	2.1×10^3
1×10^{-6}	215	1.4×10^4	141	2.2×10^3

Table **5-9**: Results of Block-diagonal one level preconditioner with elasticity coarse projection in the coarse using coefficient III defined in Figure **2-9** and load forces in Figure **2-10**.

If we compare this preconditioner with the previous preconditioners, we see an improvement in the number of iterations but the spectral condition is very high.

5.1.4 Block-diagonal one level preconditioner and elasticity coarse projection with rotations

In this case we take the previous example and modify the coarse level of the preconditioner adding rotations. We enrich the coarse spaces used in the last preconditioner. This is motivated by the fact that the elasticity matrix has a null space spanned by the rigid body motions. In particular, in two-dimensions and due to our previous construction we only need to add the rotations. Let $r = (r_x, r_y)$ be the interpolation on the fine-grid of the vector function representing the rotation. To the basis functions previously constructed we add the basis

$$[\chi_i r_x, \chi_i r_y], \tag{5-3}$$

in each neighborhood. That is,

$$M_{E,rot}^{-1} = \begin{bmatrix} M_H^{-1} & 0 \\ 0 & M_H^{-1} \end{bmatrix} + \begin{bmatrix} R_{0,rot} \\ R_{0,rot} \end{bmatrix} A_{0,E}^{-1} \begin{bmatrix} R_{0,rot} \\ R_{0,rot} \end{bmatrix}^\top,$$

with

$$A_{0,E} = \begin{bmatrix} R_{0,rot} \\ R_{0,rot} \end{bmatrix} A_E \begin{bmatrix} R_{0,rot} \\ R_{0,rot} \end{bmatrix}^\top.$$

We solve the elasticity problem using this preconditioner for different values of the contrast and forces,

$$M_{E,rot}^{-1} A_E u_E = M_{E,rot}^{-1} b_E,$$

and we obtain the results in Tables **5-10**, **5-11** and **5-12**.

- ***Coefficient without channels that reach the domain border***

	Forcing term A		Forcing term B		Forcing term C	
Coefficient	Iterations	Spectral condition	Iterations	Spectral condition	Iterations	Spectral condition
1	26	16	26	17	26	16
1×10^{-2}	34	23	34	21	33	22
1×10^{-4}	43	35	45	35	43	35
1×10^{-6}	50	40	52	40	49	40

Table **5-10**: Results of block-diagonal one level preconditioner and elasticity coarse projection with rotations using coefficient I defined in Figure **2-5** and load forces in Figure **2-6**.

- ***Coefficient with the high stiffness reach the boundary***

	Forcing term A		Forcing term B		Forcing term C	
Coefficient	Iterations	Spectral condition	Iterations	Spectral condition	Iterations	Spectral condition
1	27	18	26	17	27	19
1×10^{-2}	36	28	33	28	35	29
1×10^{-4}	37	30	34	29	36	30
1×10^{-6}	37	30	34	29	36	30

Table **5-11**: Results of block-diagonal one level preconditioner and elasticity coarse projection with rotations using coefficient II defined in Figure **2-7** and load forces in Figure **2-8**.

- ***High-contrast coefficient***

	Forcing term A		Forcing term B	
Coefficient	Iterations	Spectral condition	Iterations	Spectral condition
1	26	17	29	21
1×10^{-2}	92	2.7×10^2	81	2.4×10^2
1×10^{-4}	138	6.3×10^2	117	6.3×10^2
1×10^{-6}	130	5.4×10^2	110	5.4×10^2

Table **5-12**: Results of block-diagonal one level preconditioner and elasticity coarse projection with rotations using coefficient III defined in Figure **2-9** and load forces in Figure **2-10**.

The result for the block diagonal one level preconditioner and the elasticity coarse projection with rotations are better than the three previous ones, because it reduces the iterations and the spectral condition decreases, but if we compare to the Tables **4-1**, **4-2** and **4-3**, we see that the two levels elasticity preconditioner makes half the iterations. And the spectral condition for the new preconditioner increases for high contrast.

5.1.5 Heat coarse projection in the coarse level for the elasticity problem

In this case the coarse level of the preconditioner comes from the heat problem in equation 4-27 and the first level from elasticity in the equation 4-31. That is,

$$M_{E,1}^{-1} + \begin{bmatrix} R_0 A_0^{-1} R_0^\top \\ R_0 A_0^{-1} R_0^\top \end{bmatrix},$$

where the part corresponding to the first level is

$$M_{E,1}^{-1} r = \sum_{i=1}^{N} R_{E,i} A_{E,i}^{-1} R_{E,i}^\top r.$$

We solve the elasticity problem using this preconditioner for different values of the contrast and forces

$$M_{E,1}^{-1} + \begin{bmatrix} R_0 A_0^{-1} R_0^\top \\ R_0 A_0^{-1} R_0^\top \end{bmatrix} A_E = M_{E,1}^{-1} + \begin{bmatrix} R_0 A_0^{-1} R_0^\top \\ R_0 A_0^{-1} R_0^\top \end{bmatrix} b_E \tag{5-4}$$

and we get the results in Tables **5-13**, **5-14** and **5-15**.

- ***Coefficient without channels that reach the domain border***

	Forcing term A		Forcing term B		Forcing term C	
Coefficient	Iterations	Spectral condition	Iterations	Spectral condition	Iterations	Spectral condition
1	26	22	28	24	25	22
1×10^{-2}	44	7.5×10^2	44	7.5×10^2	45	7.5×10^2
1×10^{-4}	55	7.3×10^4	56	7.3×10^4	55	7.3×10^4
1×10^{-6}	65	7.3×10^6	65	7.3×10^6	65	7.3×10^6

Table **5-13**: Results of elasticity coarse projection in the coarse level for the elasticity problem for coefficient I defined in Figure **2-5** and load forces in Figure **2-6**.

- ***Coefficient with the high stiffness reach the boundary***

	Forcing term A		Forcing term B		Forcing term C	
Coefficient	Iterations	Spectral condition	Iterations	Spectral condition	Iterations	Spectral condition
1	27	22	28	24	28	24
1×10^{-2}	49	1.4×10^2	49	1.3×10^2	49	1.4×10^2
1×10^{-4}	50	1.7×10^2	50	1.7×10^2	50	1.7×10^2
1×10^{-6}	50	1.7×10^2	50	1.7×10^2	50	1.7×10^2

Table **5-14**: Results of elasticity coarse projection in the coarse level for the elasticity problem with coefficient II defined in Figure **2-7** and load forces in Figure **2-8**.

- ***High-contrast coefficient***

	Forcing term A		Forcing term B	
Coefficient	Iterations	Spectral condition	Iterations	Spectral condition
1	30	24	29	24
1×10^{-2}	60	87	56	82
1×10^{-4}	162	8.7×10^2	139	9.2×10^2
1×10^{-6}	174	5.6×10^3	120	2.5×10^3

Table **5-15**: Results of elasticity coarse projection in the coarse level for the elasticity problem with coefficient III defined in Figure **2-9** and load forces in Figure **2-10**.

Comparing with the previous preconditioner that so far has good results, in the tables **5-13**, **5-14** and **5-15**, we can see that the iterations increase and the spectral condition is disproportionately higher for all the contrasts.

5.1.6 Elasticity coarse projection in the coarse level for the elasticity problem

In this case we take the first level of elasticity preconditioner described in equation 4-31 and we modify the coarse level of the preconditioner,

$$M_{E,1}^{-1} + \begin{bmatrix} R_0 \\ R_0 \end{bmatrix} A_{0,E}^{-1} \begin{bmatrix} R_0 \\ R_0 \end{bmatrix}^\top,$$

where

$$A_{0,E} = \begin{bmatrix} R_0 \\ R_0 \end{bmatrix} A_E \begin{bmatrix} R_0 \\ R_0 \end{bmatrix}^\top.$$

And we solve the elasticity problem using this preconditioner

$$\left(M_{E,1}^{-1} + \begin{bmatrix} R_0 \\ R_0 \end{bmatrix} A_{0,E}^{-1} \begin{bmatrix} R_0 \\ R_0 \end{bmatrix}^\top\right) A_E u_E = \left(M_{E,1}^{-1} + \begin{bmatrix} R_0 \\ R_0 \end{bmatrix} A_{0,E}^{-1} \begin{bmatrix} R_0 \\ R_0 \end{bmatrix}^\top\right) b_E.$$

For different values of the contrast we obtain the results in Tables **5-16**, **5-17** and **5-18**.

- ***Coefficient without channels that reach the domain border***

	Forcing term A		Forcing term B		Forcing term C	
Coefficient	Iterations	Spectral condition	Iterations	Spectral condition	Iterations	Spectral condition
1	15	5.2	15	5.2	15	5
1×10^{-2}	23	12	23	12	22	12
1×10^{-4}	28	19	29	19	28	19
1×10^{-6}	33	24	34	24	32	24

Table **5-16**: Results of elasticity coarse projection in the coarse level for the elasticity problem using coefficient I defined in Figure **2-5** and load forces in Figure **2-6** .

- ***Coefficient with the high stiffness reach the boundary***

	Forcing term A		Forcing term B		Forcing term C	
Coefficient	Iterations	Spectral condition	Iterations	Spectral condition	Iterations	Spectral condition
1	15	5.2	15	5.2	15	5.2
1×10^{-2}	21	8.8	20	10	20	10
1×10^{-4}	21	9.3	20	11	20	10
1×10^{-6}	19	7.8	19	7.6	18	7

Table **5-17**: Results of elasticity coarse projection in the coarse level for the elasticity problem using coefficient II defined in Figure **2-7** and load forces in **2-8**.

- ***High-contrast coefficient***

	Forcing term A		Forcing term B	
Coefficient	Iterations	Spectral condition	Iterations	Spectral condition
1	15	5.2	15	5.2
1×10^{-2}	39	73	35	72
1×10^{-4}	81	3.6×10^2	69	3.6×10^2
1×10^{-6}	97	2.4×10^3	58	1.8×10^2

Table **5-18**: Results of elasticity coarse projection in the coarse level for the elasticity problem using coefficient defined in Figure **2-9** and load forces in Figure **2-10**.

5.1.7 Enriching the coarse space with rotations

We enrich the coarse spaces used in the last preconditioner, we constructed the bases function for the rotations described in the equation 5-3. The preconditioner enrich with rotations is,

$$M_{E,1}^{-1} + \begin{bmatrix} R_{0,rot} \\ R_{0,rot} \end{bmatrix} A_{0,E}^{-1} \begin{bmatrix} R_{0,rot} \\ R_{0,rot} \end{bmatrix}^{\top} \tag{5-5}$$

where

$$A_{0,E} = \begin{bmatrix} R_{0,rot} \\ R_{0,rot} \end{bmatrix} A_E \begin{bmatrix} R_{0,rot} \\ R_{0,rot} \end{bmatrix}^{\top}.$$

And we solve the next linear system

$$\left(M_{E,1}^{-1} + \begin{bmatrix} R_{0,rot} \\ R_{0,rot} \end{bmatrix} A_{0,E}^{-1} \begin{bmatrix} R_{0,rot} \\ R_{0,rot} \end{bmatrix}^{\top} \right) A_E u_E = \left(M_{E,1}^{-1} + \begin{bmatrix} R_{0,rot} \\ R_{0,rot} \end{bmatrix} A_{0,E}^{-1} \begin{bmatrix} R_{0,rot} \ R_{0,rot} \end{bmatrix}^{\top} \right) b_E.$$

We get the results in Tables **5-19**, **5-20** and **5-21** .

- ***Coefficient without channels that reach the domain border with coefficient***

	Forcing term A		Forcing term B		Forcing term C	
Coefficient	Iterations	Spectral condition	Iterations	Spectral condition	Iterations	Spectral condition
1	14	4.6	14	4.6	14	4.5
1×10^{-2}	21	11	22	11	20	11
1×10^{-4}	26	15	28	15	26	15
1×10^{-6}	31	19	32	19	30	19

Table **5-19**: Results of the elasticity equation with rotations in coarse spaces using coefficient I defined in Figure **2-5** and load forces in Figure **2-6**.

- ***Coefficient with the high stiffness reach the boundary***

	Forcing term A		Forcing term B		Forcing term C	
Coefficient	Iterations	Spectral condition	Iterations	Spectral condition	Iterations	Spectral condition
1	14	4.6	14	4.6	14	4.5
1×10^{-2}	18	6.2	17	6.2	17	6.1
1×10^{-4}	20	8.1	18	7.9	18	7.1
1×10^{-6}	19	7.2	19	11	18	7.7

Table **5-20**: Results of the elasticity equation with rotations in coarse spaces using coefficient II defined in Figure **2-7** and load forces in Figure **2-8**.

- ***High-contrast coefficient***

	Forcing term A			Forcing term B		
Coefficient	Iterations	Spectral condition	$\dim A_0$	Iterations	Spectral condition	$\dim A_0$
1	14	4.6	243	14	4.6	243
1×10^{-2}	30	18.4	387	28	18.3	387
1×10^{-4}	64	111.8	387	56	108.9	387
1×10^{-6}	82	374.8	387	58	140.8	387

Table **5-21**: Results of the elasticity equation with rotations in coarse spaces using coefficient III defined in Figure **2-9** and load forces in Figure **2-10**.

For the following experiments we use the enriching the coarse space with rotations preconditioner in section 5.1.7, that gave the best results to solve the elasticity equation. The enriching the coarse space with rotations preconditioner does not decrease the iterations of the preconditioner of two levels of elasticity, but is more computationally efficient because it uses the base functions of heat equation and the number of iterations is lower than in the other preconditioners presented.
In addition, we only use the high contrast coefficient, which is the most complicated coefficient to solve the elasticity equation.

5.1.8 Randomized eigenvectors approximation

In this section we analyze the random method of eigenvectors seen in [37].

We consider an abstract variational problem, where the global bilinear form is obtained by assembling local bilinear forms, see more in [17]. That is $a(u,v) = \sum_Q a_Q(R_Q u, R_Q v)$, where $a_Q(u,v)$ is a bilinear form acting on functions with supports being the coarse block Q. Define the subdomain bilinear form $a_{\omega_i}(u,v) = \sum_{Q \subset \omega_i} a_Q(u,v)$. We consider the abstract problem

$$a(u,v) = F(v) \quad \text{for all } v \in V.$$

We introduce $\{\chi_j\}$, a partition of unity subordinated to coarse-mesh blocks and $\{\xi_i\}$ a partition of unity subordinated to overlapping decomposition, see in [17]. We also define the mass bilinear form m_{ω_i} and the Rayleigh quotient $\mathcal{Q}_{abs}$ by

$$m_{\omega_i}(v,v) := \sum_{j \in \omega_i} a(\xi_i \chi_j v, \xi_i \chi_j v) \quad \text{and} \quad \mathcal{Q}_{abs}(v) := \frac{a_{\omega_i}(v,v)}{m_{\omega_i}(v,v)}.$$

The snapshot space can be obtained by dimension reduction techniques or similar computations. For example, we can consider: In each subdomain ω_i, $i = 1, \ldots, N_S$:

(1) Generate forcing terms $f_1, f_2, \ldots, f_M$ randomly ($\int_{\omega_i} f_\ell = 0$);
(2) Compute the local solutions $-\text{div}(\kappa\nabla u_\ell) = f_\ell$ with homogeneous Neumann boundary condition;
(3) Generate $W_i = \text{span}\{u_\ell\} \cup \{1, r_x, r_y\}$;
(4) Consider $\mathcal{Q}_{gm}$ with W_i in (3) and compute important modes.

The idea is to restrict the eigenvalue problem (3-5), and therefore (3-6) to the subspace W_i.

Consider the matrix U_i whose columns generate the subspace $W_i = \text{span}\{u_\ell\} \cup \{1, r_x, r_y\}$. Then we can introduce the reduced size matrices,

$$\widetilde{\mathbf{A}_{\mathbf{E}}}^{\omega_i} = U_i^T \mathbf{A_E}^{\omega_i} U_i,$$

and

$$\widetilde{\mathbf{M}}^{\omega_i} = U_i^T \mathbf{M}^{\omega_i} U_i.$$

Then, instead of (3-6) we can solve the smaller dimension eigenvalue problem

$$\widetilde{\mathbf{A}_{\mathbf{E}}}^{\omega_i} \widetilde{\psi}^{\omega_i} = \widetilde{\lambda}^{\omega_i} \widetilde{\mathbf{M}}^{\omega_i} \widetilde{\psi}^{\omega_i}. \tag{5-6}$$

As in [17] we then consider the approximations of the eigenvalues as

$$\lambda^{\omega_i} \approx \widetilde{\lambda}^{\omega_i}, \tag{5-7}$$

and the approximation of the eigenvectors as,

$$\psi^{\omega_i} \approx U_i \widetilde{\psi}^{\omega_i}. \tag{5-8}$$

We note that the eigenvalue problem (5-6) is of the size of the dimension of the space W_i (or the number of snapshots, as they are call it in [17, 9]). Therefore the size of the eigenvalue problem (5-6) is much smaller than the size of the full eigenvalue problem (3-5), see more in [37].

Heat basis

This experiment is result of applying the random method for the heat part of the preconditioner in section 5.1.7, we use 10 and 15 random vectors, see in Tables **5-22** and **5-23** for the coarse heat space in 5-5.

- Using 10 random vectors

	Forcing term A			Forcing term B		
Coefficient	Iterations	Spectral condition	$\dim A_0$	Iterations	Spectral condition	$\dim A_0$
1	24	13.0	243	24	13.8	243
1×10^{-2}	35	26.9	387	32	26.8	387
1×10^{-4}	72	111.2	387	62	111.1	387
1×10^{-6}	90	388.3	387	69	276.7	387

Table **5-22**: Elasticity coarse projection in the coarse level for the elasticity problem with rotations for coefficient III, using random eigenvectors generation with 10 random vectors.

- Using 15 random vectors

	Forcing term A			Forcing term B		
Coefficient	Iterations	Spectral condition	$\dim A_0$	Iterations	Spectral condition	$\dim A_0$
1	25	16.0	243	25	15.6	243
1×10^{-2}	34	25.9	387	33	27.0	387
1×10^{-4}	72	112.5	387	62	111.4	387
1×10^{-6}	90	388.2	387	69	276.5	387

Table **5-23**: Elasticity coarse projection in the coarse level for the elasticity problem with rotations for coefficient III, using random eigenvectors generation with 15 random vectors.

Elasticity basis

In this experiment, we use the two level additive Schwarz preconditioner for the elasticity equation defined in 4-30. We apply the random method in the first level of the elasticity preconditioner in equation 4-31. In the Tables **5-24** and **5-25** we present the results of the elasticity equation with 10 and 15 random vectors respectively.

- Using 10 random vectors

	Forcing term A			Forcing term B		
Coefficient	Iterations	Spectral condition	$\dim A_0$	Iterations	Spectral condition	$\dim A_0$
1	20	9.4	243	20	9.4	243
1×10^{-2}	32	23.7	387	30	22.9	387
1×10^{-4}	68	124.4	387	57	121.9	387
1×10^{-6}	72	141.2	387	63	141.0	387

Table **5-24**: Two-levels domain decomposition for the elasticity equation for coefficient III, using random eigenvectors generation with 10 random vectors.

- Using 15 random vectors

	Forcing term A			Forcing term B		
Coefficient	Iterations	Spectral condition	dim A_0	Iterations	Spectral condition	dim A_0
1	20	9.4	243	20	9.4	243
1×10^{-2}	32	22.6	387	30	22.8	387
1×10^{-4}	68	124.3	387	58	122.0	387
1×10^{-6}	72	141.2	387	63	141.1	387

Table **5-25**: Two-levels domain decomposition for the elasticity equation for coefficient III, using random eigenvectors generation with 15 random vectors.

After analyzing all the possible combinations between the elasticity and heat preconditioners for the elasticity problem with the high contrast coefficient, based on the number of iterations of the conjugate gradient and on the spectral condition of the conditioned matrix, we can compare the less cost preconditioners with the two-level elasticity preconditioner.

Based on the number of iterations, the best preconditioner is the two levels elasticity preconditioner because for all the coefficients and applied forces the number of iterations is lower. But we have to emphasize that the cases of the elasticity coarse projection enriched with rotations in the coarse level preconditioner presented in 5.1.7, the random eigenvectors generation with heat basis preconditioner and the random eigenvectors generation with elasticity basis preconditioner have good results for the number of iterations of the conjugate gradient for the high contrast coefficient. We also note that the spectral condition of the conditioned matrix in these cases does not increase too much compared with the two levels elasticity preconditioner, see tables **5-21**, **5-22**,**5-23**, **5-24** and **5-25**. In the next chapter we use these three preconditioners to solve topology optimization problems to test their operation.

6 Topology Optimization

Topology optimization consists in finding the efficient material distribution in different settings. The first formal work on this topic is "Generating optimal topologies in structural design using a homogenization method" (see [2]) that had a high impact on the industrial applications. Other important work of Bendsøe is a compilation of topology optimization theory, applications and the finite element code used to solve these applications in "Topology optimization" (as we can see in [3]). The more recent review can be find in [28]. Several articles have published freely available codes as in [27] and [1].

Perhaps the most popular approach to topology optimization so called the density technique, illustrated in the Figure **6-1** where the structure is discretized and the density of each element is calculated iteratively by an optimization algorithm, using multiple calls to the Finite Element solver. The result is a distribution of material density that specifies the optimal shape of the structure.

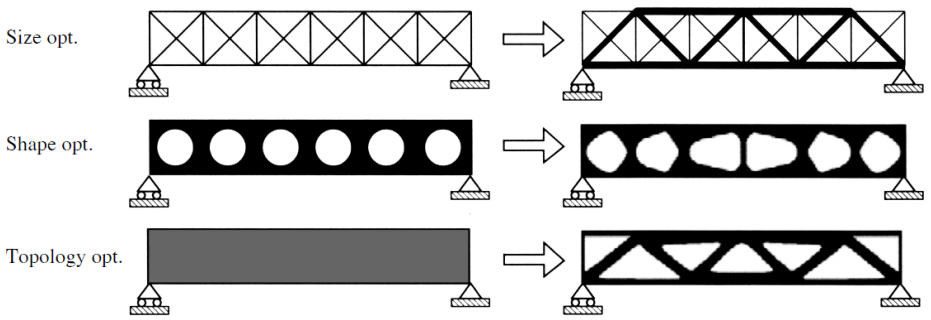

Figure **6-1**: Categories of structural optimization types for the MBB beam, original shape on left and optimized state on right. By [3, p.2].

The topology optimization goal is to improve a specified quantity of interest subject to a set of constraints. To achieve this optimal behavior we must minimize or maximize a functional that describes the desired property of the material subject to a boundary value problem which describes the physical conditions. To solve the boundary value problem the Finite Element Method is applied. For the optimization part, we use algorithms like the method of moving asymptotes (MMA) among others.

6.1 Minimum compliance design

Consider a mechanical element as a body occupying a domain Ω^{mat} which is part of a larger reference domain Ω (for a detailed exposition see [3]). We define the optimal design problem in the reference domain Ω as finding the optimal stiffness tensor $E(x)$ defined in the elasticity problem, which is variable over Ω. The minimum compliance problem can defined as,

$$\begin{cases} \min\limits_{u\in u, C} \left(\int_\Omega F : u \, d\,\Omega + \int_\Gamma \sigma_n : u \, d\, S \right) \\ \text{s.t.:} \\ \int_\Omega (C(x)(\varepsilon(u))) : \varepsilon(v) \, d\,\Omega = \int_\Omega F : v \, d\,\Omega + \int_\Gamma \sigma_n : v \, dS \text{ for all } u \in u, \\ \text{Vol}\,(\Omega^{mat}) \leq V^*, \\ C \in C_{ad} \end{cases} \tag{6-1}$$

where u is the space of kinematically admissible displacement fields, V^* is a prescribed volume of material and E_{ad} is the set of admissible stiffness tensor for our problem. To solve (6-1) we discretized the problem using FEM leading to the following discrete formulation,

$$\begin{cases} \min\limits_{u, C_e} c(u) = F^\top u \\ \text{s.t.:} \\ K(C_e)u = F, \\ \text{Vol}\,(\Omega^{mat}) \leq V^*, \\ C_e \in C_{ad} \end{cases} \tag{6-2}$$

Here u and f are the displacement and load vectors, respectively. The local stiffness matrix K depends on the stiffness C_Q in the elements $Q \in \{1, 2, \ldots, n\}$ and K the global stiffness matrix is written as:

$$K = \sum_{Q=1}^{N_Q} K_Q(C_Q),$$

where K_Q is the element stiffness matrix (see more in [3]).

6.1.1 Example: MBB Beam

Assume the following optimization problem: take a rectangular bar supported on both extremes and under a downward force in the center of the bar as we can see in Figure **6-2**.

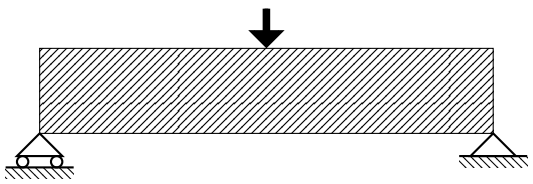

Figure **6-2**: MBB problem scheme, consider a bar supported on both extremes and under the action of a force.

We want to minimize the flexibility (or compliance) of the bar by combining two materials but reducing one of the materials to a given percentage. So the problem is recast as to determinate the best shape of the bar to achieve this objective. This problem arose from a support beam from a layout aircraft produced by Messerschmitt-Bölkow-Blohm[1], now MBB beam is the classical problem to show in topology optimization.
Usually, the problem is reduced by symmetry to the half MBB beam as shown in Figure **6-3**.

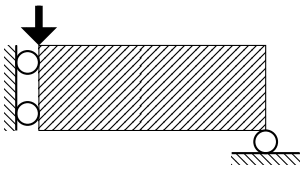

Figure **6-3**: Half MBB problem scheme, due to symmetry the MBB problem can be reduced. This means the domain is cut to the half of the original size.

To solve this problem several approaches can be taken, but historically, the evolution of methods began with *size optimization*. It is a process that relies on shrinking or enlarging parts of the structure in order to optimize it. Note that this optimization process conserves the shape of the object and allow for minimal modifications which do not change significantly the properties of the original structure.

Other popular approach is *shape optimization* which improves the last method by changing the shape of the structure in order to find the optimum value of a cost functional. But shape optimization maintains the topological properties of the structure fixed and it is unable to modify it extensively. For example, this method does not allow the creation of void parts inside the structure. The advantage of topology optimization is that it is possible to change the topological properties of the structure which provides a great flexibility in the search for the best topology.

6.2 Design Parametrization

To design an optimal structure of an isotropic material, we must determine which are the places where there are material and voids (no material), we look for a black and white design that can be manufactured using a certain amount of material.

The design should be on the Ω domain, and what we are looking for is to find Ω^{mat} the optimal set of points with material see more in [3]. The set of admissible values C_{ad} describe

[1]Messerschmitt-Bölkow-Blohm (MBB) was a German aerospace manufacturer formed as the result of several mergers in the late 1960s. Among its best-known products was the MBB Bo 105 light twin helicopter. The company was bought by DASA (Deutsche Aerospace AG) in 1989, which is now part of Airbus, from [34].

the problem defined as:

$$C_{ijk} = 1_{\Omega^{mat}} C^0_{ijkl},$$

where C_{ijkl} is the stiffness tensor, C^0_{ijkl} have the proprieties of the material and

$$1_{\Omega^{mat}} = \begin{cases} 1 & \text{if} \quad x \in \Omega^{mat}, \\ 0 & \text{if} \quad x \in \Omega / \Omega^{mat}. \end{cases}$$

The maximum volume required is,

$$\int 1_{\Omega^{mat}} = V(\Omega^{mat}) \leq V,$$

here V is a prescribed volume bound. Since the stiffness tensor, $C^0_{ijkl} \in L^\infty(\Omega)$ and we want to obtain a (0-1) result, we have to implement a penalty that turns the problem into a discrete problem.

6.2.1 Modified SIMP approach

For problem (6-1) we consider a black and white representation of the solution, for which in each element Q we assigned a physical density ρ_Q and $0 \leq \rho^p_Q \leq 1$

$$C_Q(\rho_Q) = C_{min} + \rho^p_Q (C_0 - C_{min}), \tag{6-3}$$

where C_0 is the material stiffness, C_{min} is a very small stiffness assigned to void regions in order to ensure that the global stiffness matrix is possitive definite and invertable and p is the penalty parameter (usually we use $p = 3$). The equation (6-3) is called ***modified SIMP (Solid Isotropic material with penalization).***

The minimum compliance problem (6-2) written in density terms and including the modified SIMP is:

$$\begin{cases} \min\limits_{u, C_Q} c(u) = u^\top F = \sum\limits_{Q=1}^{N_Q} C_Q(\rho_Q) u_Q^\top K_0 u_Q \\ \text{s.t.:} \\ K(C_Q)u = F, \\ C_Q(\rho_Q) = C_{min} + \rho^p_Q (C_0 - C_{min}), \qquad \forall Q \\ f_\nu(\rho_Q) = \dfrac{\sum\limits_{i \in N_Q} \rho_i v_i}{V} \leq V^*, \\ 0 \leq \rho_Q \leq 1 \end{cases} \tag{6-4}$$

That intermediate densities are unfavourable for $p = 3$ in the sense that the stiffness obtained is small compared to the cost (volume) of the material, see Figure **6-4**. For the experiments the volume constraint is active and penalty parameter $p = 3$ is big enough so that the design we get is close to $(0 - 1)$, see more in [3].

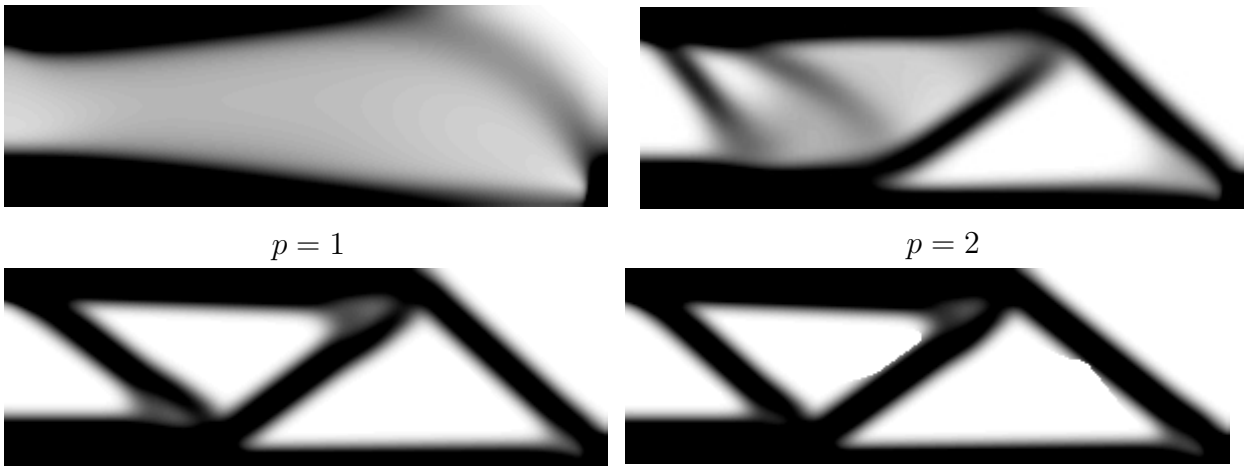

Figure **6-4**: The optimized design obtained with a variant of the 88 line code, using the modified SIMP approach for multiple penalty values p.

6.3 Solution methods

To solve a problem of topological optimization it is important to be efficient, so we use an optimization adapted with certain variables, according to the problem.

6.3.1 Conditions of optimality

For the minimum compliance problem in (6-4) can be utilized to generate efficient computational update schemes. The most common heuristic gradient based updating scheme is,

$$\rho^{K+1} = \begin{cases} \max(0, \rho_Q^K - m) & \text{if} \quad \rho_Q B_Q^\eta \leq \max(0, \rho_Q^K - m) \\ \rho_Q^K B_Q^\eta & \text{if} \quad \max(0, \rho_Q^K - m) \leq \rho_Q^K B_Q^\eta \leq \min(1, \rho_Q^K + m) \\ \min(1, \rho_Q^K + m) & \text{if} \quad \rho_Q^K B_Q^\eta \geq \min(1, \rho_Q^K + m) \end{cases} \tag{6-5}$$

Here ρ^K is the density iteration step K, η is a numerical damping efficient to stabilize the iteration,m is a positive move limit (η and m are chosen by experiment, in order to obtain convergence of the iteration), A useful value η and m is 0.5 and 0.2, respectively. And

$$B_Q^K = \frac{-\dfrac{\partial c}{\partial \rho_Q}}{\lambda \dfrac{\partial V}{\partial \rho_Q}} \tag{6-6}$$

where λ is Lagrangian multiplier, see more in [1, 3] and c is objective function.

Sensitivity analysis

To solve the topological optimization problem we are interested in analyzing the variables of the mathematical programming algorithm. The ***sensitivity analysis*** considers the displacement fields are given implicitly in terms of the design variables through the equilibrium equation and finding the derivatives of the displacements with respect to the design variables, see more in [3].
We consider the optimization problem defined in the equation (6-4), where the equilibrium equation is considered as part of the function

$$c(\rho_Q) = F^\top u,$$

To solve (6-4) we use (6-6), for which we need a gradient of the objective function, which in turn can be obtained by taking the derivative of the equilibrium equation $Ku = F$, see more in [3]. We use the adjoint method rewriting $c(\rho)$ by adding the zero function,

$$c(\rho) = F^\top u - \widetilde{u}^\top (Ku - F),$$

where $\widetilde{u}$ is any arbitrary, but fixed real vector.

$$\frac{\partial c}{\partial \rho_Q} = \left(F^\top - \widetilde{u}^\top K\right) \frac{\partial u}{\partial \rho_Q} - \widetilde{u}^\top \left(\frac{\partial K}{\partial \rho_Q} u\right),$$

when $\widetilde{u}$ satisfies the adjoint problem $F^\top = \widetilde{u}^\top K$, we can written $u = \widetilde{u}$

$$\frac{\partial c}{\partial \rho_Q} = -\widetilde{u}^\top \left(\frac{\partial K}{\partial \rho_Q} u\right)$$

and we have,

$$\frac{\partial c}{\partial \rho_Q} = -p\rho_Q^{p-1}(C_0 - C_{\min}) u^\top K_0 u. \tag{6-7}$$

And the material volume sensitivities V with respect to the element density ρ_Q are given by:

$$\frac{\partial V}{\partial \rho_Q} = 1, \tag{6-8}$$

see more in [1, 3].

6.3.2 MMA

An alternative to Optimality Criteria is the Method of Moving Asymptotes (MMA) is a method for non-linear programming in general and structural optimization, from [24] and [29] in sense that they work with a sequence of simpler approximate subproblems, see more in [3]. In each step of the iterative process, a strictly convex approximating subproblem is generated and solved. The generation of these subproblems is controlled by so called

"moving asymptotes", which may both stabilize and speed up the convergence of the general process. The Method of Moving Asymptotes allows us to solve problems with more than one constraint, without significant changes to the code, and its implementation is easy as it requires almost the same parameters as the Optimality Criteria.
In MMA the approximation or a function f of n real variables $x = (x_1, \ldots, x_n)$ around a given iteration point x^0 is,

$$f(x) \approx f(x^0) + \sum_{i=1}^{n} \left(\frac{r_i}{U_i - x_i} + \frac{s_i}{x_i - L_i} \right),$$

where the numbers r_i and s_i are chosen as (see more in [3]),

$$\begin{aligned} &\text{if } \frac{\partial f}{\partial x_i}(x^0) > 0, \qquad \text{then } r_i = (U_i - x_i^0)\frac{\partial F}{\partial x_i}(x^0) \qquad \text{and } s_i = 0, \\ &\text{if } \frac{\partial f}{\partial x_i}(x^0) < 0, \qquad \text{then } s_i = -(x_i^0 - L_i)^2\frac{\partial F}{\partial x_i}(x^0) \qquad \text{and } r_i = 0 \end{aligned}$$

where the positive numbers U_i and L_i control the range for the f approximation, this parameters give a vertical asymptotes for the optimization problem. MMA approximation of the compliance gives a subproblem after iteration step k as

$$\begin{aligned} &\min_{\rho_Q} \left((\rho^k) - \sum_{Q=1}^{N_Q} \frac{(\rho_Q^k - L_Q)^2}{\rho_Q - L_Q} \frac{\partial c}{\partial \rho_Q}(\rho^k) \right) \\ &\text{s.t.:} \\ &f_\nu(\rho_Q) = \frac{\sum_{i \in N_Q} \rho_i v_i}{V} \leq V^*, \\ &0 \leq \rho_Q \leq 1 \end{aligned} \tag{6-9}$$

The MMA is the most popular optimization method, it improves the speed of convergence and it is also more flexible than optimality criteria to add constraints, see in [3, 24] and [29].

6.4 Filtering

In topology optimization, two problems can appear, mesh dependence and checkerboard patterns. The mesh dependency can be evidenced when we refine the mesh size and the structure changes at the end of the optimization see in Figure **6-5**. And the checkerboard patterns appear due to bad numerical properties of the discretization, and then the solution does not represent optimal solution. In this section we present different filters to solve both problems.

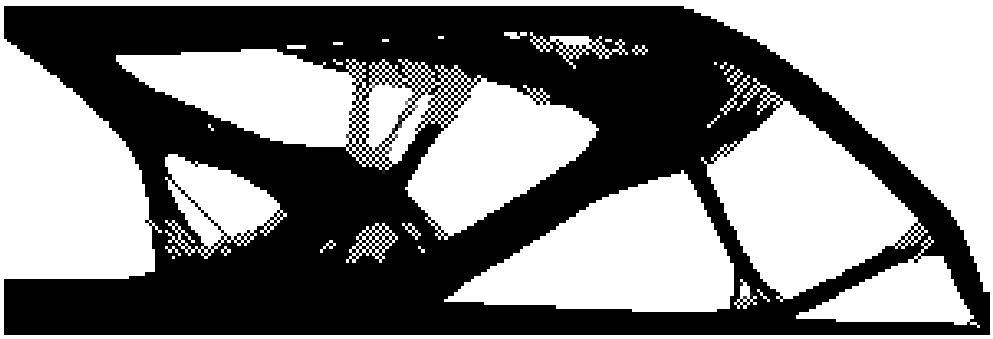

Figure **6-5**: Topology Optimization without filter.

6.4.1 Sensitivity Filter

Sensitivity filters are efficient to solve problems with the dependence of the mesh. The sensitivity filter modifies the sensitivities $\frac{\partial c}{\partial \rho_Q}$,

$$\frac{\partial c}{\partial \rho_Q} = \frac{1}{\max(\gamma, r_{\min} - \|x_i - x_Q\|) \sum_{i \in N_Q} \omega_{Q,i}} \sum_{i \in N_Q} \omega_{Q,i} \rho_i \frac{\partial c}{\partial \rho_i} \tag{6-10}$$

where γ is the small number introduced in order to avoid division by zero, N_Q is the set of element I for which the center-to-center distance $\|x_I - x_Q\|$ to element Q,

$$\omega(x_I) = r_{\min} - \|x_I - x_Q\|. \tag{6-11}$$

and $r_{\min}$ is the radius filter, which usually is equal to 0.04 times the width of the domain. In the next figures, we present some experiment in the half MBB problem with different mesh size and sensitivity filter.

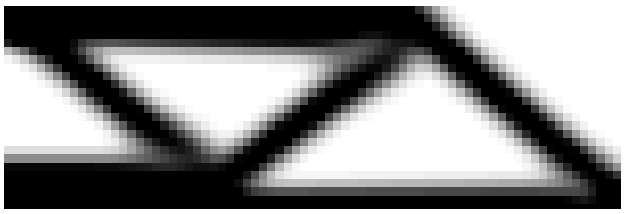

Figure **6-6**: Half MBB problem with 75×25 cells and $r_{min} = 3$.

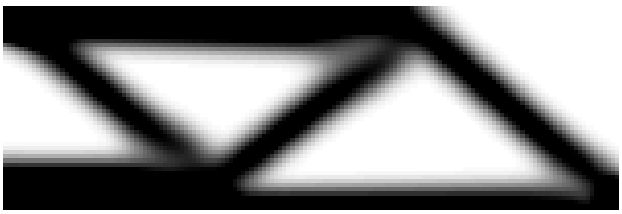

Figure **6-7**: Half MBB problem with 150×50 cells and $r_{min} = 6$.

In Figure **6-6** we take a mesh with 75×25 elements and $r_{\min} = 3$ and in Figure **6-7** we take the double elements, in both cases the topology optimization have the same results.

6.4.2 Density Filter

The most popular optimization method is density filter that will help us find the projection filter. For the optimization problem we apply conditions for the density with the modified SIMP, see more in [3]. Density filtering can be written in form of the convolution integral as:

$$\widetilde{\rho}_Q(x) = \int_\Omega \omega(x-y)\rho_Q(x),$$

where $w(x)$ is a weighting function.
The density filter can be explicitly defined as,

$$\widetilde{\rho}_Q = \frac{\sum\limits_{i \in N_Q} \omega(x_I) v_i \rho_I}{\sum\limits_{i \in N_Q} \omega(x_I) v_I}, \tag{6-12}$$

where v_I is volume in the element I and ω is defined in 6-11. And the derivative of the density filter is:

$$\frac{\partial \widetilde{\rho}_Q}{\partial \rho_j} = \frac{w(x_J) v_J}{\sum\limits_{j \in N_Q} w(x_Q) v_Q} \tag{6-13}$$

In the Figure **6-8**, we apply the density filter for the half MBB problem, and we have a structure with mesh independence.

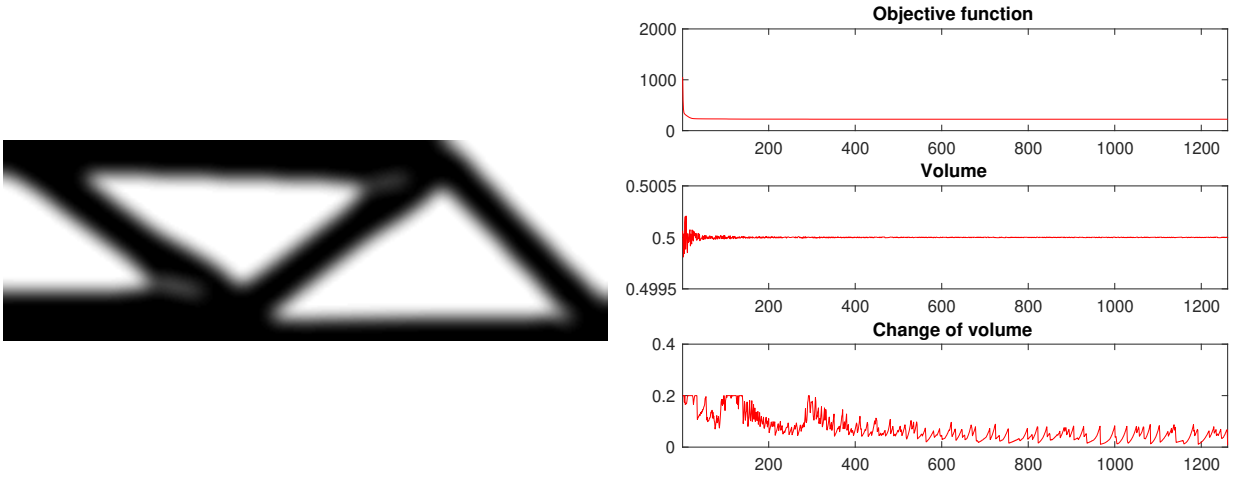

Figure **6-8**: Left: the optimized design obtained with a variant of the 88 line code, using density filter. Right: evolution of parameters during the optimization.

6.5 Projections

Implementing a filter in the optimization algorithm allows to eliminate the mesh dependency and the checkerboard patterns of the optimal structure, but the filter radius allows gray areas with intermediate density. To eliminate the gray areas and for the optimization process to be a pure black and white design, we are going to implement a filter based on projections.

Heaviside projection filtering

All filtered density values $\widetilde{\rho}_Q$ above a threshold η are projected to 1 and the values below to 0. The projected physical density $\bar{\widetilde{\rho}}_Q$ is calculated by a smooth function controlled by a projection parameter β and give as:

$$\bar{\widetilde{\rho}}_Q = \begin{cases} \eta[\exp(-\beta(1-\widetilde{\rho}_Q/\eta)) - (1-\widetilde{\rho}_Q/\eta)\exp(-\beta)] & 0 \leq \widetilde{\rho}_Q \leq \eta, \\ (1-\eta)[1-\exp(-\beta(\widetilde{\rho}_Q-\eta)/(1-\eta)) & \\ +(\widetilde{\rho}_Q-\eta)/(1-\eta)\exp(-\beta)] + \eta & \eta \leq \widetilde{\rho}_Q \leq 1. \end{cases} \tag{6-14}$$

The expression 6-14 can be substitute the previous expression for smoothed Heaviside function as:

$$\bar{\widetilde{\rho}}_Q = \frac{\tanh(\beta\eta) + \tanh(\beta(\widetilde{\rho}_Q - \eta))}{\tanh(\beta\eta) + \tanh(\beta(1-\eta))}, \tag{6-15}$$

with $\beta \to \infty$. The physical density $\bar{\widetilde{\rho}}_Q$ is used to compute the stiffness matrix and the sensitivities are:

$$\frac{\partial c}{\partial \rho_Q} = \sum_{I \in N_Q} \sum_{J \in N_I} \frac{\partial c}{\partial \bar{\widetilde{\rho}}_Q} \frac{\partial \bar{\widetilde{\rho}}_Q}{\partial \widetilde{\rho}_Q} \frac{\partial \widetilde{\rho}_Q}{\partial \widetilde{\rho}_Q}$$

In the Figure **6-9** we have the optimal design for the half-MBB problem with Heaviside projection filter.

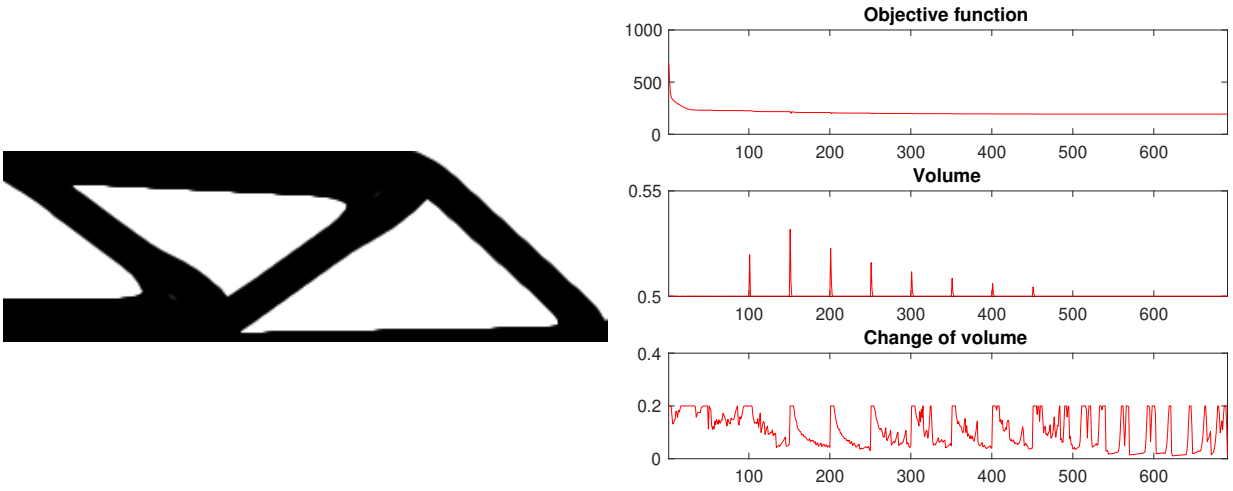

Figure **6-9**: Left: the optimized design obtained with a variant of the 88 line code, using Heaviside approach. Right: evolution of parameters during the optimization.

For the different η values we can find multiple projections. Two important projections are obtained by replacing $\eta = 0$ and $\eta = 1$ in equation 6-14, resulting in the dilatation and erosion operators respectively.

Dilate operator

The dilate operator in this discrete form is a max-operator i.e. the physical density of the element Q takes the maximum of the densities in the neighborhood N_Q. But this form is not applicable in topology optimization, for that we take the continuous form of the dilate operator like a Heaviside function approximated as:

$$\bar{\tilde{\rho}}_Q^{\,d} = 1 - \exp(\beta\rho_Q)_Q + \rho_Q \exp(-\beta). \tag{6-16}$$

Erode operator

The erode operator in this discrete form is a min-operator i.e. the physical density of element Q takes the minimum of the densities in the neighborhood N_Q. But this form is not applicable in topology optimization, for that we take the continuous form of the erode operator like a Heaviside function approximated as:

$$\bar{\tilde{\rho}}_Q^{\,e} = \exp(\beta(1 - \rho_Q)) + (1 - \rho_Q)\exp(-\beta). \tag{6-17}$$

The threshold projections for $\eta = 1$ and $\eta = 0$ result in the high contrast filtered designs, and we use the dilate and erode operator to reformulate the design problem in the next section, see more in [32].

6.6 Experiments of topology optimization

Experiment 1

For the first experiment, we take a square plane with homogeneous Dirichlet boundary condition and distributed force over the domain, as in Figure **6-10**. This is not a physically realistic experiment but is a good example to test preconditioners as the topology optimization result is a highly complex design.

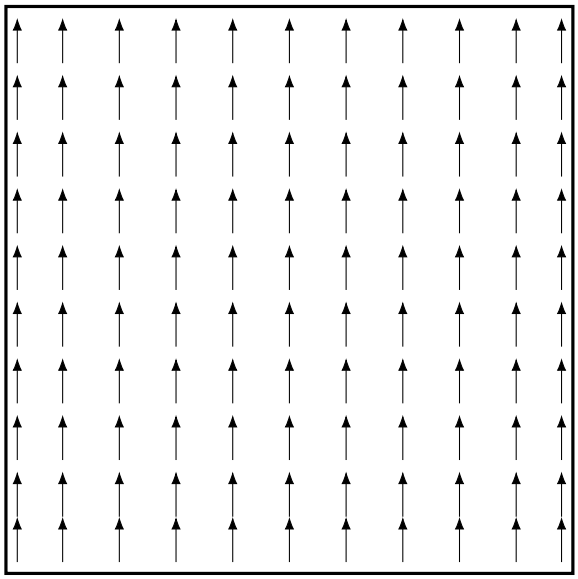

Figure **6-10**: Square plane with homogeneous Dirichlet boundary condition and distributed force over the domain.

We use the topology optimization code with the MMA optimizer and the density filter to solve the topology optimization problem in Figure **6-10**. In addition, the volume fraction is 0.3, the SIMP penalty is 3, the artificial Young's modulus assigned to void regions is $E_{min} = 10^{-3}$, see [1], and the filter radius is $r_{min} = 3$.

Table **6-1** has the results of the topology optimization for the elasticity equation with different preconditioners. We use a conjugate gradient method tolerance of 1×10^{-6} with a fine mesh of size 10×10 and coarse mesh 10×10. For the two levels elasticity preconditioner, the random preconditioner with heat basis, and the random preconditioner with elasticity basis, the maximum number of eigenvectors in each subdomain is $\lambda_{\max} = 4$. We use coarse basis recalculation as in [37] and [26]. The iterations count is for the topology optimization algorithm.

Method	Iterations	Objective Function	Coarse calculations
Without preconditioner	107	54.8158	—
Two-levels elasticity preconditioner	107	54.8158	17
Two-levels elasticity random preconditioner	107	54.8158	17
Two-levels heat preconditioner	107	54.8158	17
Two-levels heat random preconditioner	107	54.8158	16

Table **6-1**: Results of the topology optimization reusing the coarse basis calculations.

In the Table **6-1**, we see how all the tested methods achieve, in the same number of iterations, the same objective function value. In Figure **6-11**, we see the result of the topology optimization for all cases.

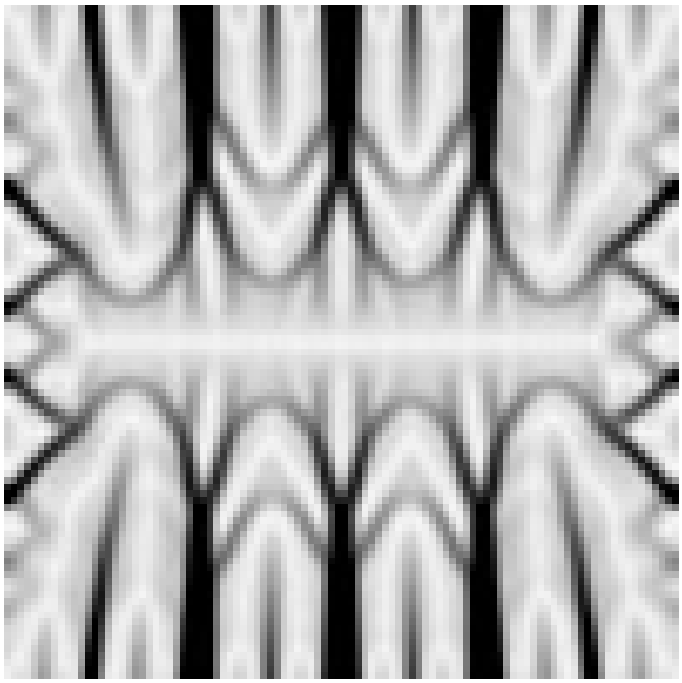

Figure **6-11**: Topology optimization of the elasticity equation, see problem scheme in Figure **6-10**.

In the Figures **6-12**, **6-13**, **6-14** and **6-15** we have the evolution of the objective function, the volume fraction, the volume change in the optimization, the iterations of the preconditioned conjugate gradient in each step of the optimization, the size of the coarse space, and (in the blue points) the steps of the optimization in which the coarse space is calculated.

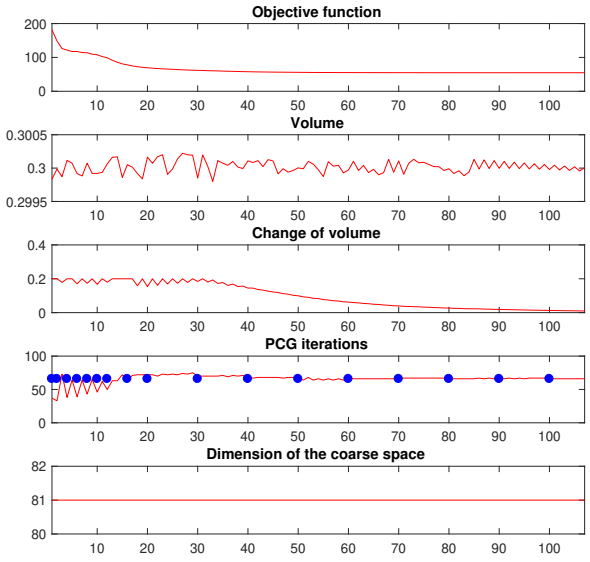

Figure **6-12**: Evolution of parameters in the topology optimization with a two levels elasticity preconditioner.

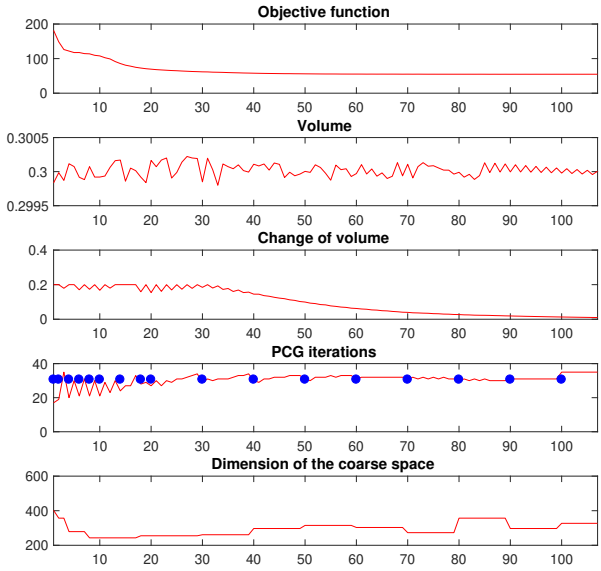

Figure **6-13**: Evolution of parameters in the topology optimization using a preconditioner with heat basis in the coarse space.

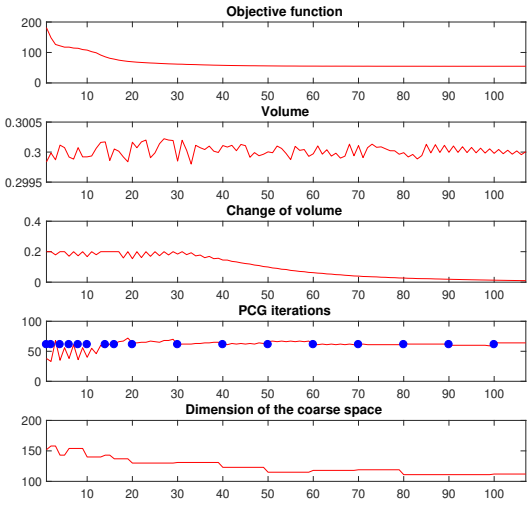

Figure **6-14**: Evolution of parameters in the topology optimization using a random preconditioner with elasticity basis.

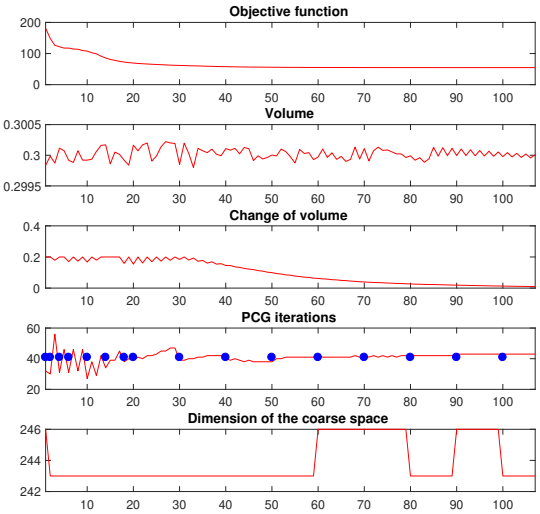

Figure **6-15**: Evolution of parameters in the topology optimization using a random preconditioner with heat basis.

We can see in Figures **6-12**, **6-13**, **6-14** and **6-15** how the first three parameters evolve in the same way for all the cases. We can also see how PCG iterations vary a lot in the first optimization steps due to the variations in the design. As optimization iterations advance

the PCG iterations stabilize. In the bottom plot we have the dimension of the coarse space.

Experiment 2

In this experiment, we take a square plane with homogeneous Dirichlet boundary condition and two fix bars over the domain with nine load forces in each, as in Figure **6-16**.

We use the topology optimization code with the MMA optimizer and the density filter to solve the topology optimization problem in Figure **6-16**. In addition, the volume fraction is 0.5, the SIMP penalty is 3, the artificial Young's modulus assigned to void regions is $E_{min} = 10^{-3}$, see [1], and the filter radius is $r_{min} = 3$.

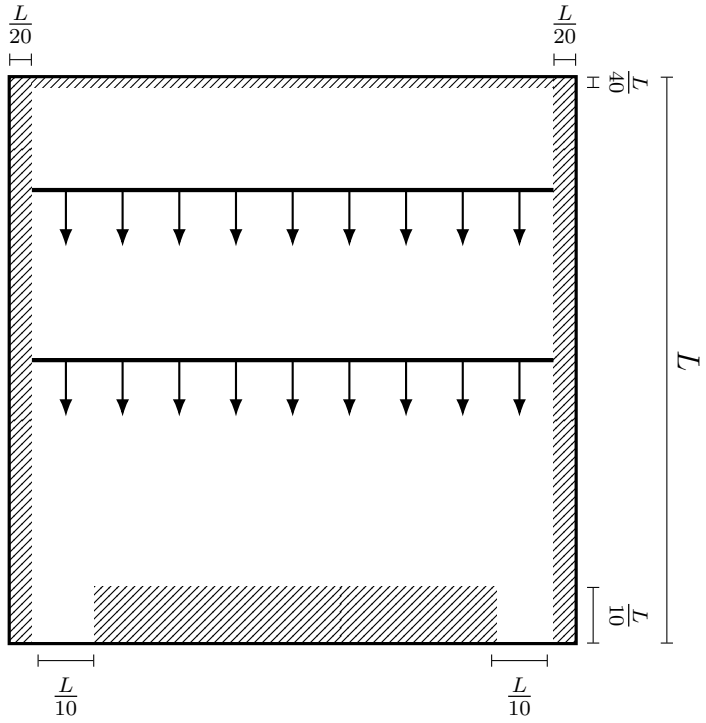

Figure **6-16**: Square plane with homogeneous Dirichlet boundary condition and two fix bars over the domain with nine load forces in each.

Table **6-2** has the results of the topology optimization for the elasticity equation with different preconditioners, for example **6-16**. We use a conjugate gradient method tolerance of 1×10^{-6} with a fine mesh of size 10×10 and coarse mesh 10×10. For the two levels elasticity preconditioner, the random preconditioner with heat basis, and the random preconditioner with elasticity basis, the maximum number of eigenvectors in each subdomain is $\lambda_{\max} = 4$, in the random preconditioner we take two different λ values, (9 and 12), and 15 snapshots. We

use coarse basis recalculation as in [37] and [26]. The iterations count is for the topology optimization algorithm.

Method	**Iterations**	**Objective Function**	**Coarse calculations**
Without preconditioner	300	0.180 651	—
Two-levels elasticity preconditioner	300	0.180 631	22
Two-levels elasticity random preconditioner	300	0.180 861	19
Two-levels heat preconditioner	300	0.180 720	16
Two-levels heat random preconditioner	300	0.180 721	17

Table **6-2**: Results of the topology optimization reusing the coarse basis calculations.

In the Table **6-2**, we see how all the tested methods achieve, in the same number of iterations, the same objective function value. In Figure **6-17**, we see the result of the topology optimization for all cases.

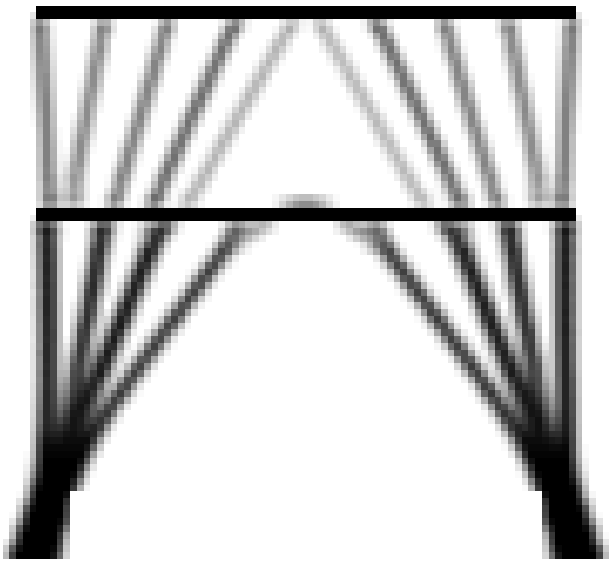

Figure **6-17**: Topology optimization of the elasticity equation, see problem scheme in Figure **6-16**.

We can see in Figures **6-18**, **6-19**, **6-20** and **6-21** how the first three parameters evolve in the same way for all the cases. We can also see how PCG iterations vary a lot in the first optimization steps due to the variations in the design. As optimization iterations advance the PCG iterations stabilize. In the bottom plot we have the dimension of the coarse space.

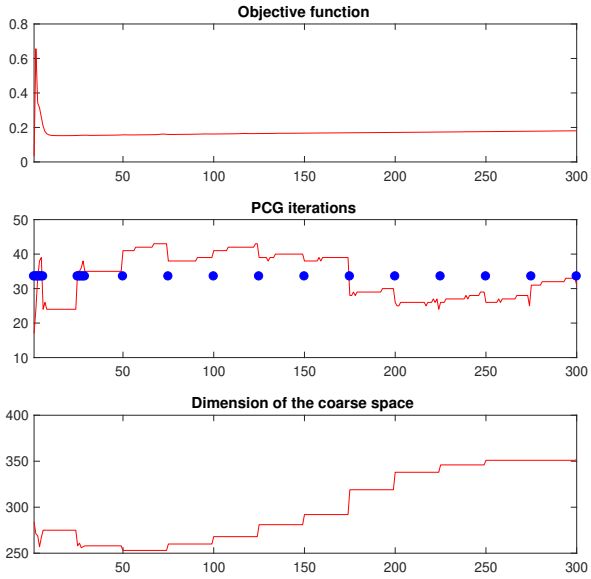

Figure **6-18**: Evolution of parameters in the topology optimization of the elasticity equation with a two levels elasticity preconditioner.

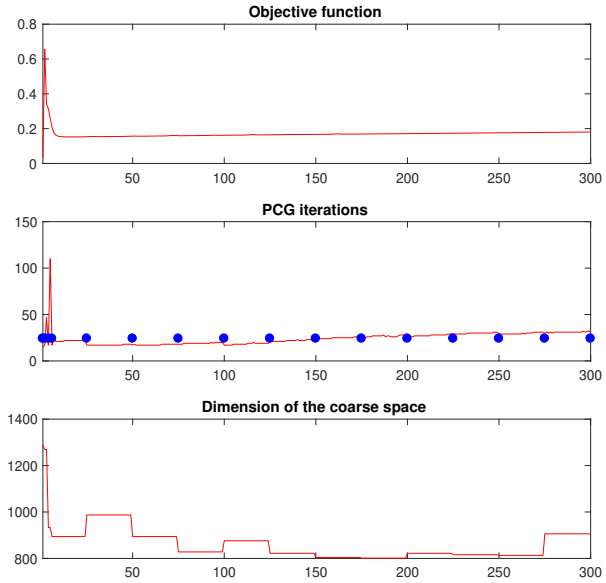

Figure **6-19**: Evolution of parameters in the topology optimization using a preconditioner with heat basis in the coarse space.

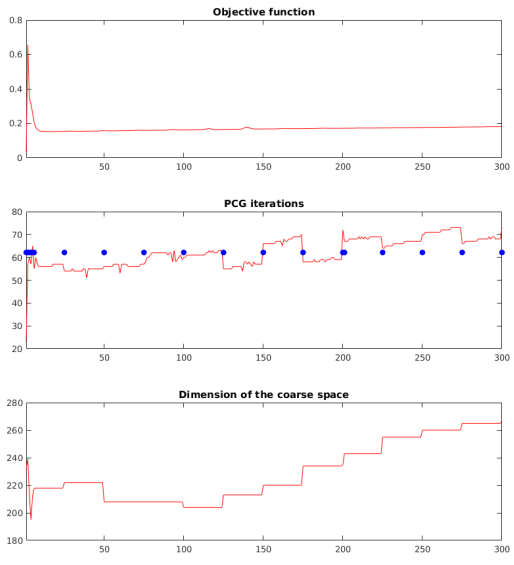

Figure **6-20**: Evolution of parameters in the topology optimization using a random preconditioner with elasticity basis.

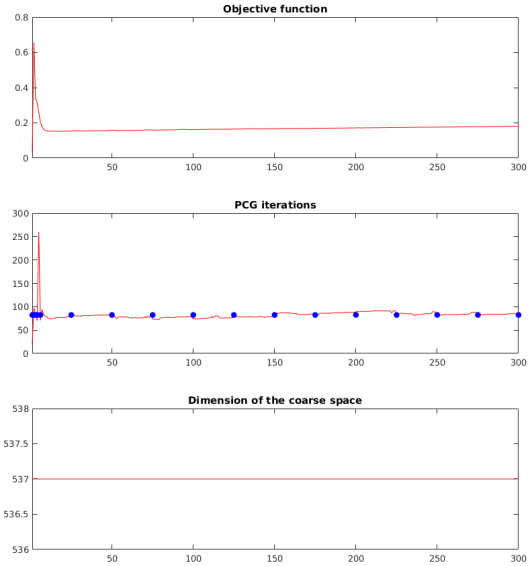

Figure **6-21**: Evolution of parameters in the topology optimization using a random preconditioner with heat basis.

7 Conclusions and recommendations

7.1 Conclusions

Topology optimization is important to solve multiple problems in the industry. To solve this type of problems we have to take a fine mesh to capture all the detail of the material distribution which makes the convergence of the state problem at every iteration extremely expensive. The use of preconditioners in this work shows that we can decrease the solver time in such topology optimization problems.

The two-levels elasticity preconditioner constructed in chapters three and four shows the decrease in the number of iterations of the conjugate gradient to solve the elasticity equation, which improves the calculation time in each step of the minimization in the topology optimization problem. We must bear in mind that the calculation time of the basis that constitute the coarse space has a significant computational cost. The presented alternative is to build lower cost preconditioners that mix heat preconditioners with elasticity. These preconditioners require less computational cost because the heat equation has half the parameters as the elasticity equation in two dimensions and also the two-levels heat preconditioner has a good performance in heat topology optimization for problems, see more in [37, 26].

After testing several combinations of the heat preconditioner with the elasticity preconditioner we obtained three possible preconditioners for the elasticity equation, elasticity coarse projection in the coarse space enriching with rotations preconditioner, randomized eigenvectors with heat basis preconditioner and randomized eigenvectors with elasticity basis preconditioner. In topology optimization we tested in different experiments we obtained good results for all preconditioners, re-utilization coarse basis, which means that we can apply this type of preconditioners to reduce the number of iterations in the conjugate gradient in each step of the minimization of the topology optimization and the calculation time in high contrast problems.

7.2 Recommendations

In a future work, we could formally prove that the preconditioner with a second level formed by heat basis enriched with rotations, randomized eigenvectors with heat and elasticity basis

are a viable option to solve the elasticity equation for topology optimization problems and and support the numerical results presented in this work.

For topology optimization problems we can select a suitable criterion for the calculation of the number of basis in each subdomain for the elasticity equation, as it is in the heat equation presented in [37]. We could also experiment with the re-utilization the coarse basis lower the computational cost.

Bibliography

[1] E. Andreassen, A. Clausen, M. Schevenels, B.S. Lazarov, and O. Sigmund. Efficient topology optimization in MATLAB using 88 lines of code. *Structural and Multidisciplinary Optimization*, 2010.

[2] Martin Philip Bendsøe and Noboru Kikuchi. Generating optimal topologies in structural design using a homogenization method. *Computer Methods in Applied Mechanics and Engineering*, 71(2):197 – 224, 1988.

[3] M.P. Bendsøe and O. Sigmund. *Topology Optimization: Theory, Methods, and Applications*. Springer Berlin Heidelberg, 2003.

[4] V. Calo, Y. Efendiev, J. Galvis, and G. Li. Randomized oversampling for generalized multiscale finite element methods. *Multiscale Modeling & Simulation*, 14(1):482–501, 2016.

[5] Y. Efendiev and J. Galvis. Domain decomposition preconditioner for multiscale high-contrast problems. In *Proceedings of DD19*, 2009.

[6] Y. Efendiev and J. Galvis. Eigenfunctions and multiscale methods for Darcy problems. Technical report, ISC, Texas A& M University, 2010.

[7] Y. Efendiev and J. Galvis. A domain decomposition preconditioner for multiscale high-contrast problems. In Y. Huang, R. Kornhuber, O. Widlund, and J. Xu, editors, *Domain Decomposition Methods in Science and Engineering XIX*, volume 78 of *Lect. Notes in Comput. Science and Eng.*, pages 189–196. Springer-Verlag, 2011.

[8] Y. Efendiev and J. Galvis. Domain decomposition preconditioner for multiscale high-contrast problems. In Y. Huang, R. Kornhuber, O. Widlund, and J. Xu, editors, *Domain Decomposition Methods in Science and Engineering XIX*, volume 78 of *Lecture Notes in Computational Science and Engineering*, pages 189–196, Berlin, 2011. Springer-Verlag.

[9] Y. Efendiev, J. Galvis, and T. Hou. Generalized multiscale finite element methods. *Journal of Computational Physics*, 251:116–135, 2013.

[10] Y. Efendiev, J. Galvis, G. Li, and M. Presho. Generalized multiscale finite element methods. oversampling strategies. *International Journal for Multiscale Computational Engineering, accepted*, 2013.

[11] Y. Efendiev, J. Galvis, and X. H. Wu. Multiscale finite element methods for high-contrast problems using local spectral basis functions. *Journal of Computational Physics*, 230(4):937–955, 2011.

[12] Y. Efendiev and T.Y. Hou. *Multiscale Finite Element Methods: Theory and Applications*. Surveys and Tutorials in the Applied Mathematical Sciences. Springer New York, 2009.

[13] Yalchin Efendiev, Juan Galvis, and Xiao-Hui Wu. Multiscale finite element methods for high-contrast problems using local spectral basis functions. *Journal of Computational Physics*, 230(4):937 – 955, 2011.

[14] J. Galvis. *Introdução aos Métodos de Decomposição de Domínio*. IMPA, 2009.

[15] J. Galvis and Y. Efendiev. Domain decomposition preconditioners for multiscale flows in high contrast media. *SIAM J. Multiscale Modeling and Simulation*, 8:1461–1483, 2010.

[16] J. Galvis and Y. Efendiev. Domain decomposition preconditioners for multiscale flows in high contrast media. reduced dimension coarse spaces. *SIAM J. Multiscale Modeling and Simulation*, 8:1621–1644, 2010.

[17] Juan Galvis, Eric Chung, Yalchin Efendiev, and Wing Tat Leung. On overlapping domain decomposition methods for high-contrast multiscale problems, 05 2017.

[18] Juan Galvis and Yalchin Efendiev. Domain decomposition preconditioners for multiscale flows in high-contrast media. *Multiscale Modeling & Simulation*, 8(4):1461–1483, 2010.

[19] I. Gustafsson and G. Lindskog. On parallel solution of linear elasticity problems. part ii: Methods and some computer experiments. *Numerical Linear Algebra with Applications*, 9(3):205–221, 2002.

[20] Ivar Gustafsson and Gunhild Lindskog. On parallel solution of linear elasticity problems: Part i: theory. *Numerical Linear Algebra with Applications*, 5(2):123–139, 1998.

[21] Axel Kaselow. The Stress Sensitivity Approach: Theory and Application, 2004.

[22] Boyan S. Lazarov. Topology optimization using multiscale finite element method for high-contrast media. In Ivan Lirkov, Svetozar Margenov, and Jerzy Waśniewski, editors, *Large-Scale Scientific Computing*, pages 339–346, Berlin, Heidelberg, 2014. Springer Berlin Heidelberg.

[23] Boyan S. Lazarov, Fengwen Wang, and Ole Sigmund. Length scale and manufacturability in density-based topology optimization. *Archive of Applied Mechanics*, 86(1):189–218, Jan 2016.

[24] M.J.H. Meijboom. *Topology optimization of dynamic problems*. DCT rapporten. Technische Universiteit Eindhoven, 2003. DCT 2003.108.

[25] A. Samuelsson and N.E. Wiberg. *Finite Element Method: Basics*. Studentlitteratur, 1998.

[26] S. Serrano, M. Zambrano, B. Lazarov, and J. Galvis. Fast multiscale contrast independent preconditioner for linear elastic topology optimization problems. In preparation.

[27] O. Sigmund. A 99 line topology optimization code written in matlab. *Structural and Multidisciplinary Optimization*, 21(2):120–127, Apr 2001.

[28] Ole Sigmund and Kurt Maute. Topology optimization approaches. *Structural and Multidisciplinary Optimization*, 48(6):1031–1055, Dec 2013.

[29] Krister Svanberg. The method of moving asymptotes a new method for structural optimization. *International Journal for Numerical Methods in Engineering*, 24(2):359–373, 1987.

[30] Andrea Toselli and Olof B. Widlund. *Domain Decomposition Methods*. Science, 2006.

[31] A.C. Ugural and S.K. Fenster. *Advanced Strength and Applied Elasticity*. Pearson Education, 2003.

[32] Fengwen Wang, Boyan Stefanov Lazarov, and Ole Sigmund. On projection methods, convergence and robust formulations in topology optimization. *Structural and Multidisciplinary Optimization*, 43(6):767–784, Jun 2011.

[33] K. Washizu. *Variational Methods in Elasticity and Plasticity*. 01. Elsevier Science & Technology, 1974.

[34] Wikipedia. Messerschmitt-Bölkow-Blohm — Wikipedia, The Free Encyclopedia, 2017. [Online; accessed 16-October-2017].

[35] Wikipedia. Norma matricial — Wikipedia, La enciclopedia libre, 2018. [Online; accessed 16-April-2018].

[36] J. Galvis Y. Efendiev and P. Vassilevski. Spectral element agglomerate algebraic multigrid methods for elliptic problems with high-contrast coefficients. In Y. Huang, R. Kornhuber, O. Widlund, and J. Xu, editors, *Domain Decomposition Methods in Science and Engineering XIX*, volume 78 of *Lecture Notes in Computational Science and Engineering*, pages 407–414. Springer-Verlag, 2011.

[37] M. Zambrano. *Topology Optimization Problems for the Heat Equation*. Masters thesis, Universidad Nacional de Colombia, 2019.